Ann. N.Y. Acad. Sci. ISSN 0077-8923

ANNALS OF THE NEW YORK ACADEMY OF SCIENCES
Issue: *Building the Knowledge Base for Climate Resiliency*

Appendix II: NPCC 2015 Technical Details

A. Climate observations and projections: Methods and analyses[a]

Contents

A.1 Observed extreme events
A.2 Global climate models (GCMs)
A.3 Climate projections

A.1 Observed extreme events

Temperature. Hot days, heat waves, and cold days in Central Park (1900–2013) based on maximum temperatures at or above 90°F, 100°F, at or above 90°F for three consecutive days, and minimum temperatures at or below 32°F (see Fig. A.1).

Precipitation. Heavy precipitation events in Central Park (1900–2013) based on daily precipitation at or above 1, 2, and 4 inches (see Fig. A.2).

Tropical storms and hurricanes. See Table A.1.

A.2 Global climate models

See Table A.2 for a list of the global climate models used in the NPCC 2015 report.

A.3 Climate projections

Methods for 2100 projections. Projections for 2100 require a different approach from the 30-year timeslices (10-year for sea level rise) that are centered on the 2020s, 2050s, and 2080s, which are what the New York City Panel on Climate Change (NPCC) traditionally uses. The primary difference is that because the vast majority of climate model simulations end in 2100, it is not possible to make a projection for the 30-year timeslice (10-year for sea level rise) centered on the year 2100.

Given this model availability constraint, the NPCC considered the alternate approaches listed below to generate projections for 2100. Both approaches share one thing in common: they involve adding a linear trend to the final timeslice (2080s for temperature and precipitation, 2090s for sea level rise), and extrapolating that trend to 2100. The final period linear trend (FPLT) is for 2085 to 2099 for temperature and precipitation, and 2095 to 2099 for sea level rise. The NPCC also considered quadratic trends as well, but determined that over the short time periods used for the trends, a linear approach produced comparable results. The two used approaches are:

1. Add each representative concentration pathway (RCP) ensemble mean FPLT to the final timeslice projections for the corresponding RCP, and calculate the four distribution points (i.e., 10th, 25th, 75th, and 90th percentiles).
2. Add the FPLT from each individual model and RCP to the final timeslice for the corresponding model and RCP, and then calculate the four distribution points (i.e., 10th, 25th, 75th, and 90th percentiles).

Approaches 1 and 2 were averaged to generate projections for 2100 (Table A.3).

It is also important to note that uncertainties are inherently much greater for the end of the century than the mid-century. For example, the RCP runs do not sample all the possible carbon and other biogeochemical cycle feedbacks associated with climate change. Even the few Earth System Models in the Coupled Model Intercomparison Project (CMIP5) used by the NPCC2 may underestimate the potential for increased methane and carbon releases from the Arctic under extreme warming scenarios. More generally, the potential for surprises increases further into the future one considers, such as technological innovations that could remove carbon from the atmosphere.

Maps of ensemble mean annual temperature and precipitation change. Figures A.3 and A.4 demonstrate that the mean temperature and

[a]This Appendix provides technical details for New York City Panel of Climate Change 2015 Report, Chapter 1: Climate Observations and Projections.

doi: 10.1111/nyas.12670

Ann. N.Y. Acad. Sci. 1336 (2015) 116–150

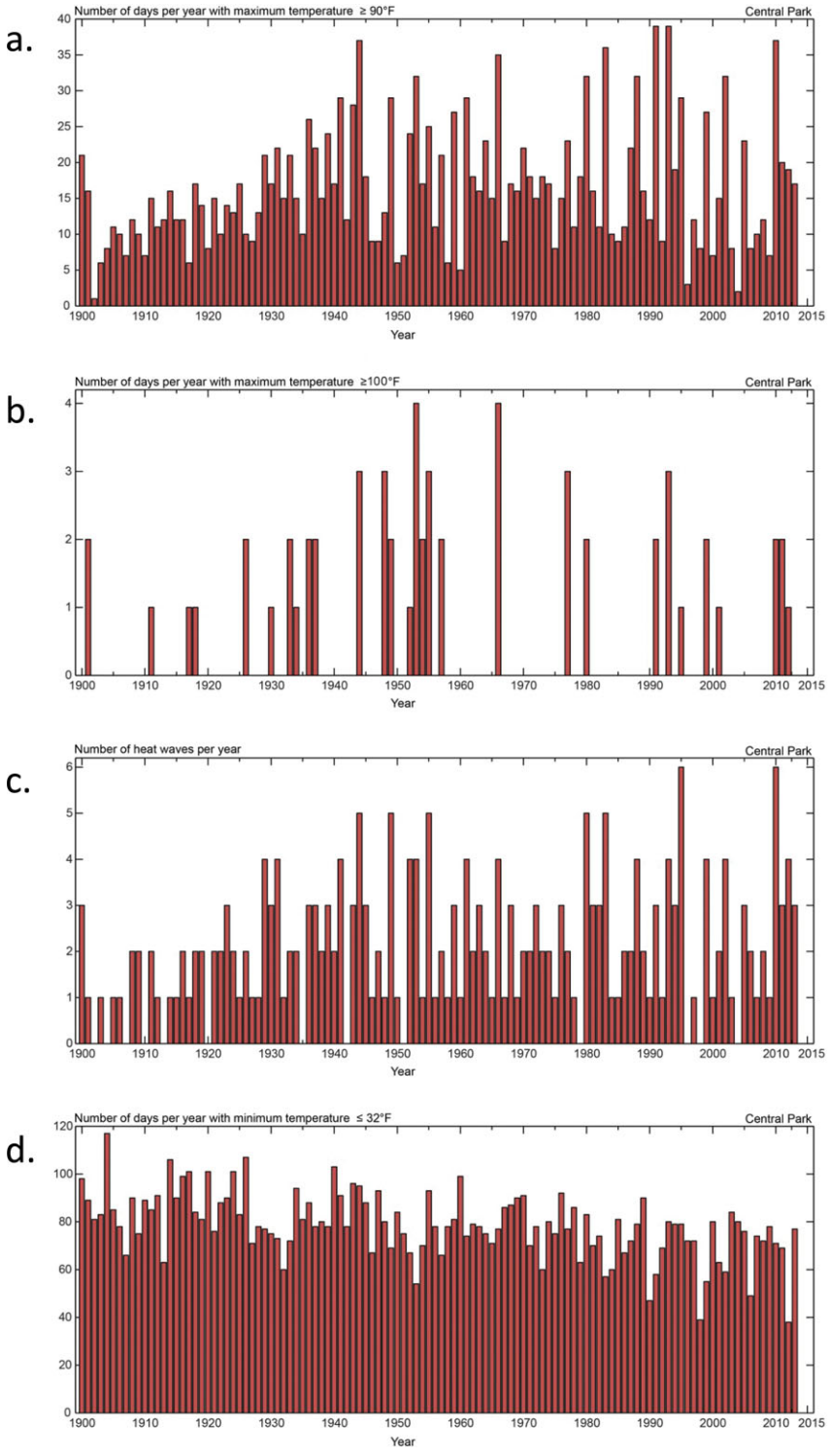

Figure A.1. Observed extreme temperature events (1900–2013): (a) maximum temperatures at or above 90°F; (b) maximum temperatures at or above 100°F; (c) heat waves (at or above 90°F for three consecutive days); and (d) minimum temperatures at or below 32°F.

Table A.1. Dates and major impacts from tropical storms and hurricanes that struck in New York metropolitan area

Date	Name	Category[a]	Central pressure[b,c]	Wind speed[b,c]	Notes
September 23, 1815	Great September Gale of 1815	3		(155)	
September 3, 1821	Norfolk and Long Island Hurricane	3	975 (970)	110 (130)	Only direct strike on New York City. Surge of 13 ft in 1 hour. Flooded parts of lower Manhattan as far north as Canal Street.
September 15, 1858	New England Storm	1	979 (976)	85 (100)	
September 8, 1869	Eastern New England Storm	2	963 (950)	100 (115)	
August 23, 1893	Midnight Storm	1	986 (952)	85 (115)	Flooded southern Brooklyn and Queens.
September 21, 1938	Long Island Express/New England Storm	3	945 (935)	110 (160)	Killed ~700 people. Storm surge of 10–12 feet on Long Island.
September 15, 1944	Great Atlantic Hurricane of 1944	1	965 (943)	80 (140)	Landfall over central Long Island.
August 31, 1954	Carol	2	975 (970)	100 (100)	Wind gusts between 115 and 125 mph over eastern Long Island.
September 12, 1960	Donna	2–3	965 (932)	110 (160)	Storm surge of 11 ft. Second highest recorded water level at the Battery (7.22 ft NAVD88). Lower Manhattan to West & Cortland Streets flooded nearly waist deep.
September 21, 1961	Esther	3	978 (927)	115 (145)	Minor flooding and power outages disrupted transportation on Long Island.
June 22, 1972	Agnes	TS – 1	980 (977)	70 (85)	Caused significant flooding.
August 10, 1976	Belle	1	980 (957)	85 (120)	Landfall on Long Island with wind gusts over 95 mph.
September 27, 1985	Gloria	2	951 (920)	105 (145)	Wind gusts over 110 mph. Struck at low tide with 5.45 ft water level (NAVD88).
August 19, 1991	Bob	2	962 (950)	105 (115)	Eye passed just east of Long Island.
September 16, 1999	Floyd	TS – 1	974 (921)	70 (155)	Major inland flooding with 24-hour rainfall totals between 10 and 15 inches in upstate New Jersey and New York.

Continued

Table A.1. *Continued*

Date	Name	Category[a]	Central pressure[b,c]	Wind speed[b,c]	Notes
August 28, 2011	Irene	TS	965 (942)	65 (120)	Center passed over Coney Island; 3–6 ft surge. Major inland flooding upstate NY and New England.
October 29, 2012	Sandy	PTS[d]–1	946 (941)	80 (115)	Major coastal flooding and power outages in New York City, New Jersey, and Long Island coasts. Record maximum water level of 11.28 ft above NAVD88 at the Battery.

NOTE: The above-mentioned storms have been selected based on their tracks and impacts on the New York metropolitan area. No single metric (i.e., location of landfall within a given distance of the city) was used to determine what storms to include.

[a]Category (based on the Saffir–Simpson Scale) is the estimated strength of the storm as it impacted the New York City area.

[b]Minimum central pressure (in millibars (mb)) and maximum wind speed (in miles per hour (mph)).

[c]The central pressure and wind speed at the time the storm impacted the area; the numbers in parenthesis are the storm's most intense observation(s).

[d]PTS, posttropical storm. The term posttropical is used in National Weather Service advisory products to refer to any closed low-pressure system that no longer qualifies as a tropical cyclone (TC). However, such systems can continue carrying heavy rains and damaging winds. Post-TCs can be either frontal (extratropical) or nonfrontal lows.

SOURCE: Unisys Hurricane Archive (http://weather.unisys.com/hurricane/).

precipitation projections for the New York metropolitan region are part of a larger regional pattern. Shown are the national and regional changes in temperature and precipitation for the 2050s relative to 1971–2000. These changes are averaged across the 35 GCMs under RCP4.5 (top) and RCP 8.5 (bottom); while the two RCPs differ in the amount of changes projected, the spatial pattern across the United States is similar for both RCPs. Because these maps represent an average across 35 models, they obscure the substantial variations from one model to another that are evident in Table A.2.

Temperature. New York City's proximity to the coast is projected to lead to approximately 0.5°F less warming than in the interior regions of the Northeast. The map also reveals that the Northeast is expected to experience slightly more warming than the mid-Atlantic.

Precipitation. Precipitation projections also show very little spatial variation across the Northeastern United States. However, the map does reveal a tendency for slightly greater precipitation increases to the north of New York City near the Canadian border, and slightly smaller increases in the mid-Atlantic region.

Seasonal and monthly projections. Throughout the 21st century, projected warming is comparable in each of the four seasons for the New York metropolitan region (Tables A.4 and A.5). As the century progresses, precipitation increases become highest during the winter season (Tables A.6 and A.7); for both the 2050s and the 2080s, winter is the only season where the 10th percentile projections show projected increases. This indicates that during the other three seasons, precipitation decreases cannot be ruled out.

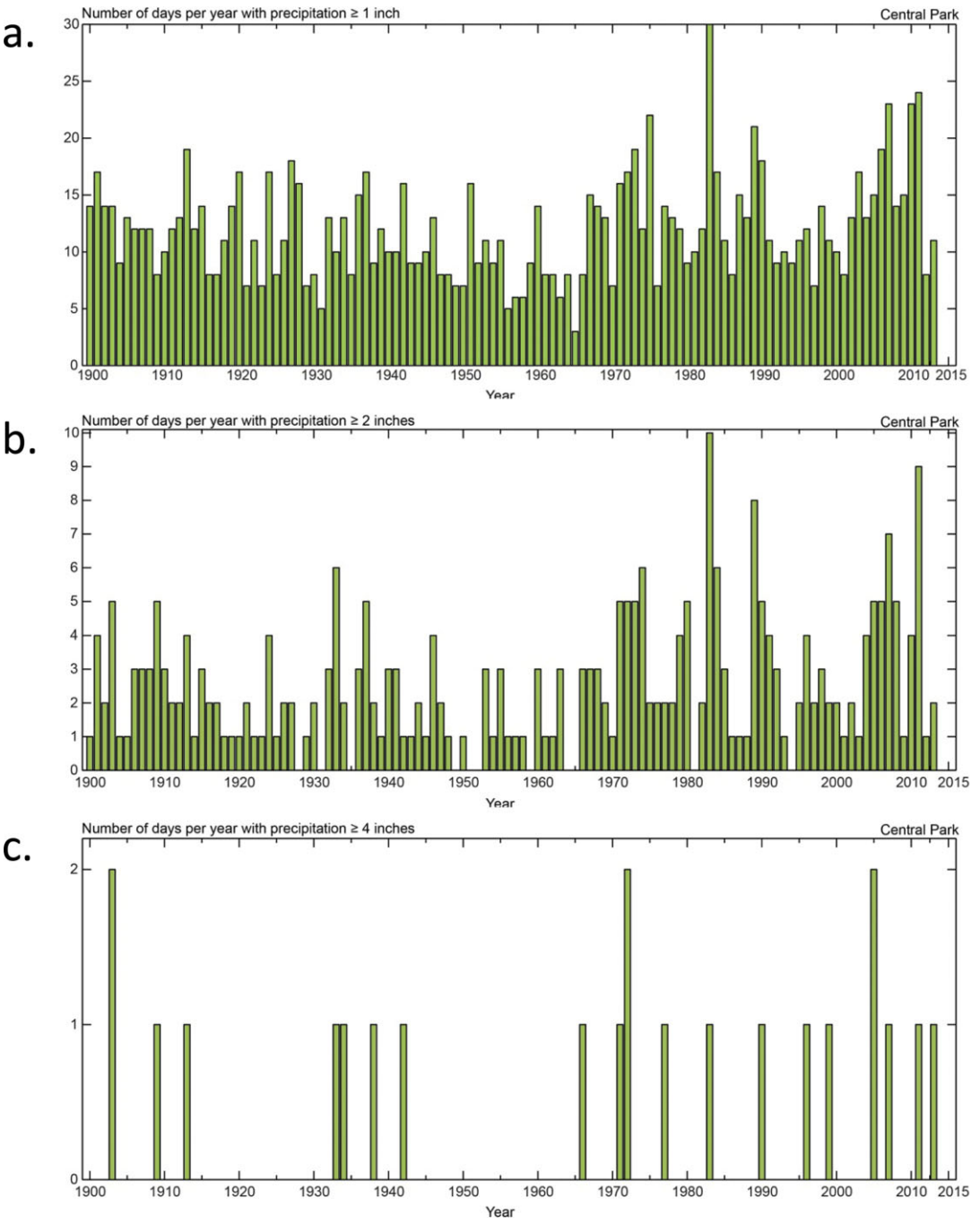

Figure A.2. Observed extreme precipitation events (1900–2013): (a) daily precipitation at or above 1 inch; (b) daily precipitation at or above 2 inches; and (c) daily precipitation at or above 4 inches.

Ann. N.Y. Acad. Sci. 1336 (2015) 116–150 © 2015 New York Academy of Sciences.

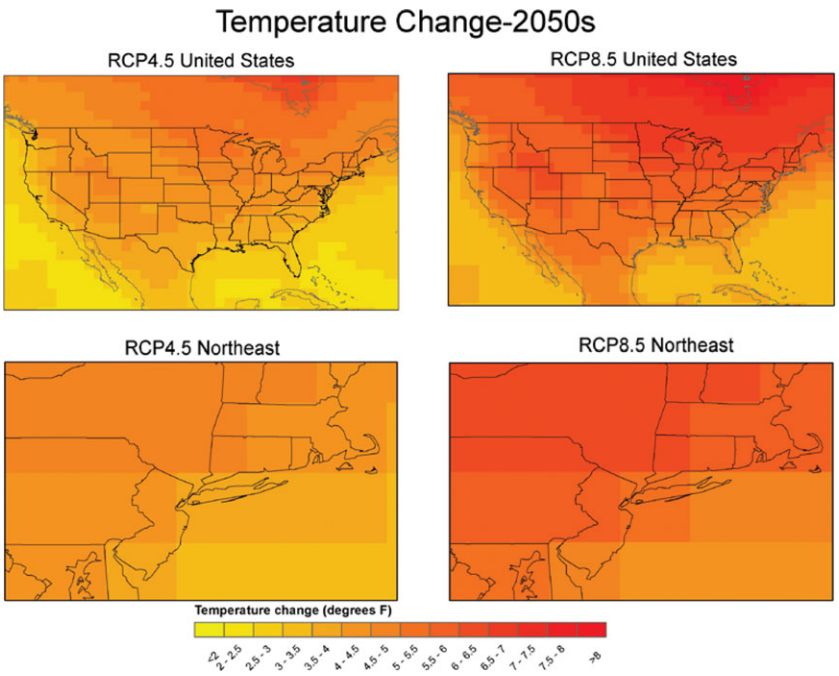

Figure A.3. Annual temperature changes in the 2050s.

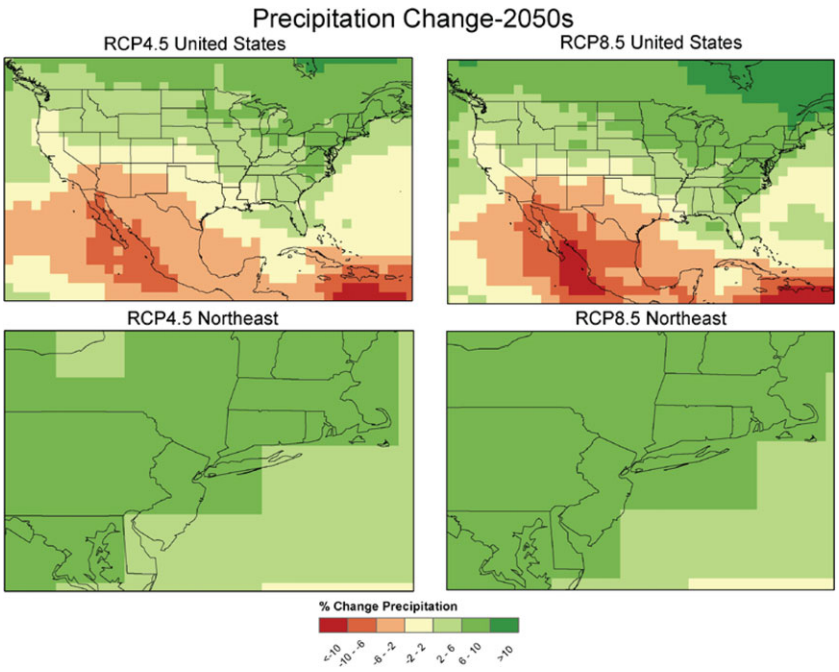

Figure A.4. Annual precipitation changes in the 2050s.

Table A.2. IPCC AR5 global climate models (GCMs) used by the NPCC2

Modeling center	Institute ID	Model name	Atmospheric resolution (lat° × lon°)
Commonwealth Scientific and Industrial Research Organization (CSIRO) and Bureau of Meteorology (BOM), Australia	CSIRO – BOM	ACCESS1.0	1.25 × 1.875
		ACCESS1.3	1.25 × 1.875
Beijing Climate Center, China Meteorological Administration	BCC	BCC-CSM1.1	2.8 × 2.8
		BCC-CSM1.1 (m)	1.1 × 1.1
College of Global Change and Earth System Science, Beijing Normal University	GCESS	BNU-ESM	2.8 × 2.8
Canadian Centre for Climate Modelling and Analysis	CCCMA	CanESM2	2.8 × 2.8
National Center for Atmospheric Research	NCAR	CCSM4	0.9 × 1.25
Community Earth System Model Contributors	NSF-DOE-NCAR	CESM1(BGC)	0.9 × 1.25
		CESM1(CAM5)	0.9 × 1.25
Centro Euro-Mediterraneo per l Cambiamenti Climatici	CMCC	CMCC-CM	0.75 × 0.75
		CMCC-CMS	1.9 × 1.9
Centre National de Recherches Météorologiques/Centre Européen de Recherche et Formation Avancée en Calcul Scientifique	CNRM-CEFRACS	CNRM-CM5	1.4 × 1.4
Commonwealth Scientific and Industrial Research Organization in collaboration with Queensland Climate Change Centre of Excellence	CSIRO-QCCE	CSIRO-Mk3.6.0	1.9 × 1.9
LASG, Institute of Atmospheric Physic, Chinese Academy of Sciences and CESS, Tsinghua University	LASG-CESS	FGOALS-g2	2.8 × 2.8
The First Institute of Oceanography, SOA, China	FIO	FIO-ESM	2.8 × 2.8
NOAA Geophysical Fluid Dynamics Laboratory	NOAA GFDL	GFDL-CM3	2.0 × 2.5
		GFDL-ESM2G	2.0 × 2.5
		GFDL-ESM2M	2.0 × 2.5
NASA Goddard Institute for Space Studies	NASA GISS	GISS-E2-H	2.0 × 2.5
		GISS-E2-R	2.0 × 2.5
National Institute of Meteorological Research/Korea Meteorological Administration	NIMR/KMA	HadGEM2-AO	1.25 × 1.875

Continued

Table A.2. *Continued*

Modeling center	Institute ID	Model name	Atmospheric resolution (lat° × lon°)
Met Office Hadley Centre (additional HadGEM2-ES realizations contributed by Instituto Nacional de Pesquisas Espaciais)	MOHC (additional realizations by INPE)	HadGEM2-CC	1.25 × 1.875
		HadGEM2-ES	1.25 × 1.875
Institute for Numerical Mathematics	INM	INM-CM4	1.5 × 2.0
Institut Pierre-Simon Laplace	IPSL	IPSL-CM5A-LR	1.9 × 3.75
		IPSL-CM5A-MR	1.3 × 2.5
		IPSL-CM5B-LR	1.9 × 3.75
Japan Agency for Marine-Earth Science and Technology, Atmosphere and Ocean Research Institute (The University of Tokyo), and National Institute for Environmental Studies)	MIROC	MIROC-ESM	2.8 × 2.8
		MIROC-ESM-CHEM	2.8 × 2.8
Atmosphere and Ocean Research Institute (The University of Tokyo), National Institute for Environmental Studies, and Japan Agency for Marine-Earth Science and Technology	MIROC	MIROC5	1.4 × 1.4
Max Planck Institute for Meteorology	MPI-M	MPI-ESM-MR	1.9 × 1.9
		MPI-ESM-LR	1.9 × 1.9
Meteorological Research Institute	MRI	MRI-CGCM3	1.1 × 1.1
Norwegian Climate Centre	NCC	NorESM1-M	1.9 × 2.5
		NorESM1-ME	1.9 × 2.5

Note: This table provides information about the 35 GCMs used by the NPCC2. The 35 models were developed by 22 modeling centers (left column). Some centers support multiple GCMs, and/or versions (for example, some institutions conducted multiple simulations at varying spatial resolutions) of their GCM.

Table A.3. NPCC2 2100 projections for temperature, precipitation, and sea level rise

	Low estimate (10th percentile)	Middle range (25th to 75th percentile)	High estimate (90th percentile)
(a) Temperature projections for 2100[a]			
Approach 1	+4.5°F	+6.0 to 10.4°F	+11.9°F
Approach 2	+3.9°F	+5.5 to 10.3°F	+12.3°F
2100 Projections (average of Approaches 1 and 2)	+4.2°F	+5.8 to 10.4°F	+12.1°F
(b) Precipitation projections for 2100[b]			
Approach 1	−1%	+2 to +14%	+18%
Approach 2	−11%	−5 to +24%	+32%
2100 Projections (average of Approaches 1 and 2)	−6%	−1 to +19%	+25%
(c) Sea-level rise projections for 2100[c,d]			
Approach 1	7 inches	9 to 18 inches	24 inches
Approach 2	6 inches	9 to 19 inches	26 inches
Model-based component average	6 inches	9 to 18 inches	25 inches
2100 Total SLR projections (average of Approaches 1 and 2)	15 inches	22 to 50 inches	75 inches

[a]Based on 35 global climate models (GCMs) and two representative concentration pathways (RCPs). Projections are relative to the 1971–2000 base period.
[b]Based on 35 GCMs and two RCPs. Projections are relative to the 1971–2000 base period.
[c]Based on 24 GCMs and two RCPs. Projections are relative to the 2000–2004 base period.
[d]Rows 1, 2, and 3 are for model-based sea level rise components only; the final row shows row three plus all other sea level change components.

Table A.4. NPCC2 projected seasonal temperature changes (°F)

	Low estimate (10th percentile)	Middle range (25th to 75th percentile)	High estimate (90th percentile)
(a) 2020s			
Winter	1.4°F	2.0°F to 3.2°F	3.7°F
Spring	1.2°F	1.6°F to 2.7°F	3.1°F
Summer	1.8°F	2.1°F to 3.1°F	3.3°F
Fall	1.9°F	2.3°F to 3.2°F	3.6°F
(b) 2050s			
Winter	3.1°F	4.2°F to 6.0°F	6.8°F
Spring	2.7°F	3.6°F to 5.2°F	6.4°F
Summer	3.1°F	4.3°F to 5.8°F	6.6°F
Fall	3.6°F	4.3°F to 5.7°F	6.8°F
(c) 2080s			
Winter	3.9°F	5.6°F to 8.8°F	10.5°F
Spring	3.7°F	4.7°F to 7.9°F	8.9°F
Summer	4.1°F	4.9°F to 9.5°F	10.5°F
Fall	3.9°F	5.5°F to 9.2°F	10.8°F

NOTES: Winter, December to February; Spring, March to May; Summer, June to August; Fall, September to November. Based on 35 GCMs and two representative concentration pathways. Projections are relative to the 1971–2000 base period.

Model-based range of outcomes (distribution) for temperature changes (°F) in New York City, relative to the 1971–2000 base period for the 2020s, 2050s, and 2080s. Projections are based on 35 GCMs and 2 representative concentrations pathways.

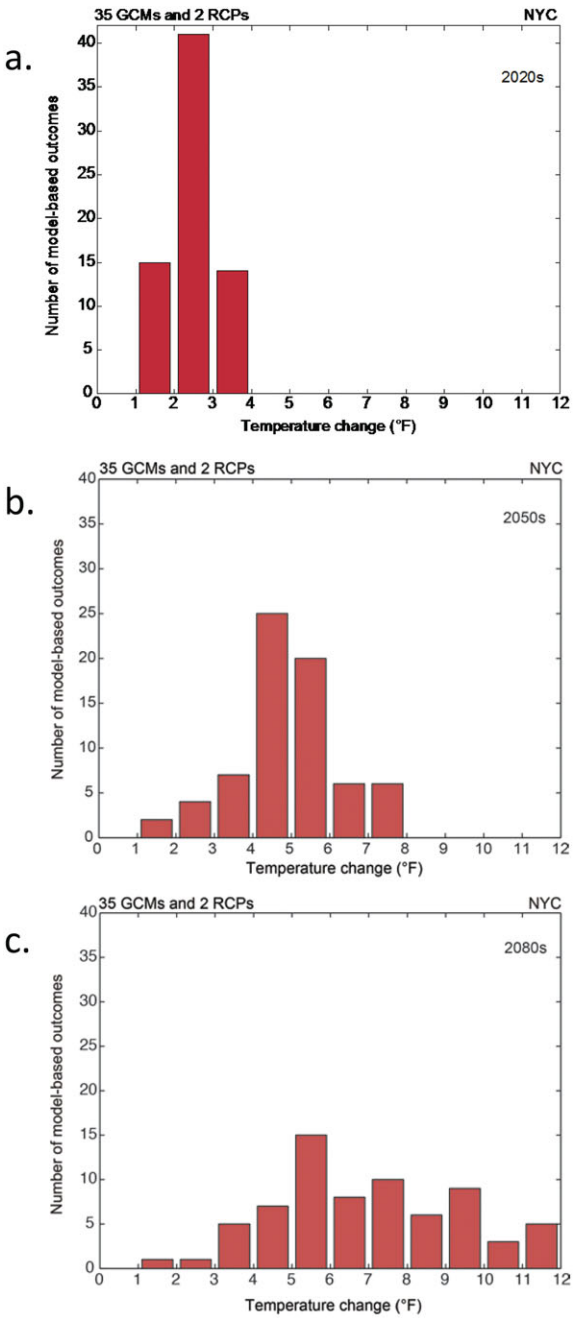

Figure A.5. Model-based range of outcomes (distribution) of projected temperature changes: (a) 2020s, (b) 2050s, and (c) 2080s.

Table A.5. Projected monthly temperature changes (°F)

	Low estimate (10th percentile)	Middle range (25th to 75th percentile)	High estimate (90th percentile)
(a) 2020s			
January	0.9°F	1.6°F to 3.6°F	4.4°F
February	0.8°F	1.6°F to 2.9°F	4.0°F
March	0.3°F	1.3°F to 2.7°F	3.6°F
April	1.1°F	1.5°F to 2.6°F	3.4°F
May	0.9°F	1.4°F to 2.9°F	3.5°F
June	1.0°F	1.7°F to 2.8°F	3.3°F
July	1.4°F	2.0°F to 3.0°F	3.3°F
August	1.5°F	2.2°F to 3.1°F	3.5°F
September	1.5°F	2.3°F to 3.2°F	3.7°F
October	1.2°F	2.0°F to 3.2°F	3.6°F
November	1.1°F	1.8°F to 3.2°F	3.8°F
December	0.6°F	1.8°F to 3.5°F	4.3°F
(b) 2050s			
January	2.9°F	3.9°F to 6.1°F	7.0°F
February	2.8°F	3.6°F to 5.7°F	6.7°F
March	2.6°F	3.6°F to 5.2°F	6.4°F
April	2.5°F	3.3°F to 5.1°F	6.5°F
May	2.4°F	3.2°F to 5.3°F	6.4°F
June	2.5°F	3.8°F to 5.9°F	6.3°F
July	2.9°F	4.1°F to 5.9°F	6.8°F
August	3.2°F	4.3°F to 6.1°F	7.0°F
September	3.3°F	4.4°F to 6.2°F	7.0°F
October	3.0°F	4.1°F to 5.9°F	6.8°F
November	3.2°F	3.9°F to 5.6°F	6.6°F
December	2.8°F	3.7°F to 6.1°F	7.0°F
(c) 2080s			
January	3.4°F	5.6°F to 8.9°F	10.7°F
February	3.5°F	5.4°F to 8.4°F	10.0°F
March	3.0°F	4.5°F to 7.4°F	8.8°F
April	3.6°F	4.7°F to 7.9°F	9.4°F
May	3.4°F	4.6°F to 8.0°F	9.2°F
June	3.3°F	4.7°F to 8.6°F	9.9°F
July	3.6°F	5.0°F to 9.3°F	10.4°F
August	4.1°F	5.1°F to 9.6°F	11.3°F
September	4.2°F	5.3°F to 9.6°F	11.0°F
October	3.7°F	4.9°F to 9.0°F	11.0°F
November	3.1°F	4.9°F to 8.4°F	9.9°F
December	3.6°F	5.3°F to 8.3°F	10.6°F

NOTE: Based on 35 GCMs and two representative concentration pathways. Projections are relative to the 1971–2000 base period.

Table A.6. Projected seasonal precipitation changes (%)

	Low estimate (10th percentile)	Middle range (25th to 75th percentile)	High estimate (90th percentile)
(a) 2020s			
Winter	−3%	+1% to +12%	+20%
Spring	−3%	+1% to +9%	+15%
Summer	−5%	−1% to +11%	+15%
Fall	−5%	−2% to +7%	+10%
(b) 2050s			
Winter	+2%	+7% to +18%	+24%
Spring	−1%	+3% to +12%	+18%
Summer	−9%	−5% to +11%	+18%
Fall	−2%	+1% to +10%	+14%
(c) 2080s			
Winter	+4%	+10% to +25%	+33%
Spring	−1%	+4% to +15%	+21%
Summer	−10%	−5% to +18%	+23%
Fall	−7%	−1% to +11%	+18%

NOTES: Winter, December to February; Spring, March to May; Summer, June to August; Fall, September to November. Based on 35 GCMs and two representative concentration pathways. Projections are relative to the 1971–2000 base period.

Model-based range of outcomes (distribution) for precipitation changes (%) in New York City, relative to the 1971–2000 base period for the 2020s, 2050s, and 2080s. Based on 35 GCMs and 2 representative concentrations pathways.

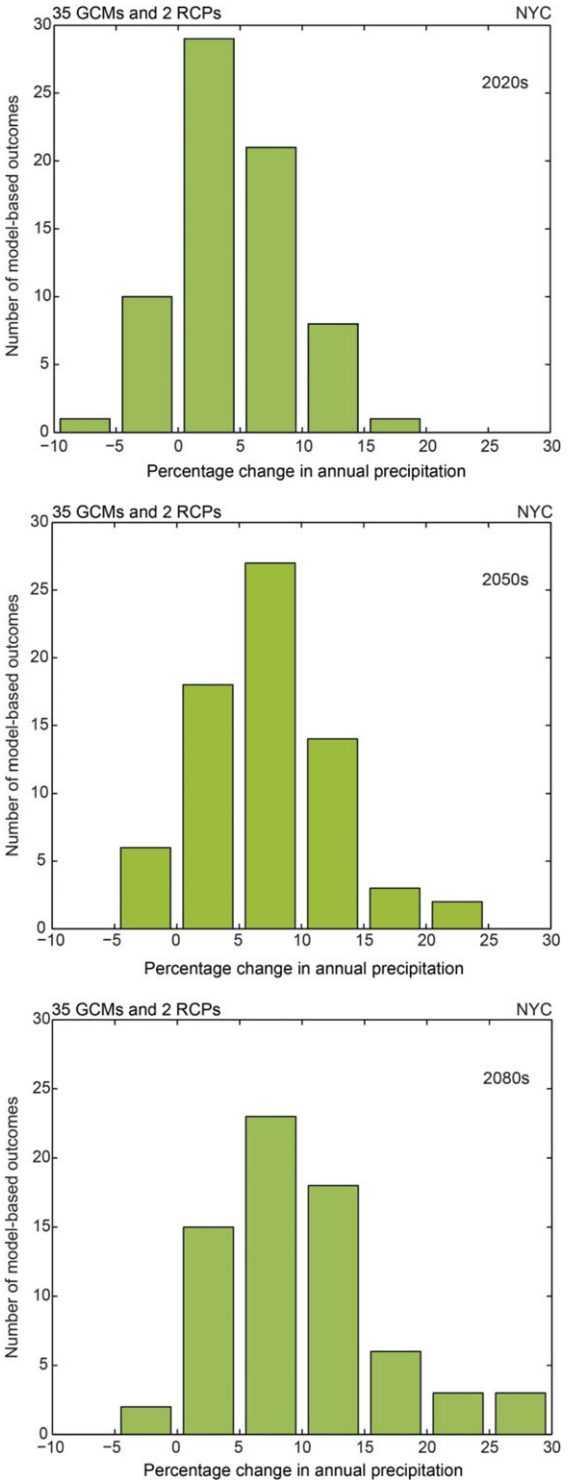

Figure A.6. Model-based range of outcomes (distribution) of projected precipitation changes: (a) 2020s, (b) 2050s, and (c) 2080s.

Table A.7. Projected monthly precipitation changes (%)

	Low estimate (10th percentile)	Middle range (25th to 75th percentile)	High estimate (90th percentile)
(a) 2020s			
January	−8%	−1% to +14%	26%
February	−9%	−2% to +16%	31%
March	−7%	−1% to +12%	19%
April	−12%	−4% to +11%	18%
May	−13%	−6% to +10%	20%
June	−14%	−4% to +9%	18%
July	−12%	−4% to +12%	20%
August	−7%	+1% to +13%	20%
September	−18%	−11% to +7%	14%
October	−19%	−7% to +12%	19%
November	−9%	−4% to +12%	21%
December	−6%	−1% to +12%	20%
(b) 2050s			
January	−4%	+1% to +25%	+35%
February	−4%	+2% to +26%	+36%
March	−3%	+1% to +18%	+25%
April	−5%	−1% to +14%	+26%
May	−10%	−5% to +11%	+17%
June	−14%	−5% to +13%	+18%
July	−14%	−9% to +10%	+23%
August	−13%	−4% to +14%	+26%
September	−20%	−8% to +11%	+16%
October	−17%	−6% to +14%	+22%
November	−5%	−1% to +18%	+23%
December	−8%	+4% to +19%	+23%
(c) 2080s			
January	−4%	+7% to +28%	+40%
February	−4%	+5% to +28%	+44%
March	−1%	+5% to +22%	+27%
April	−10%	+2% to +19%	+25%
May	−10%	−1% to +14%	+22%
June	−14%	−2% to +15%	+20%
July	−16%	−9% to +19%	+32%
August	−19%	−9% to +20%	+35%
September	−16%	−8% to +10%	+22%
October	−20%	−9% to +9%	+23%
November	−10%	−2% to +21%	+29%
December	−5%	+5% to +26%	+31%

NOTES: Based on 35 GCMs and two representative concentration pathways. Projections are relative to the 1971–2000 base period.

B. Sea level rise observations and projections: methods and analyses[b]

Contents

B.1 NPCC2 sea level rise methods and projections
B.2 Ocean changes
B.3 Ice mass change
B.4 Vertical land movements—glacial isostatic adjustment (GIA)
B.5 Anthropogenic land water storage

This section describes the New York City Panel on Climate Change (NPCC2) methodology for projecting future sea level rise in New York City.

B.1 NPCC2 sea level rise methods and projections

The regionalized sea level projection methodology used in NPCC (2010) and Horton *et al.* (2010) is updated here in NPCC2. Individual sea level rise components are described in Chapter 2, NPCC 2015. NPCC2 sea level projections do not comprise the full range of possible sea level rise contributions, but rather present the estimated 10th, 25th, 75th, and 90th percentile sea level contributions by component; the sum of components at each percentile is used to generate a total sea level rise projection for each percentile. As noted in Chapter 2 (NPCC, 2015), this approach neglects correlations between sea level rise components, which could influence the robustness of the projections.[c]

The cumulative sea level change S_{TOT} (at a given likelihood) in New York City is equal to:

$$S_{TOT} = S_{OCEAN} + S_I + S_{GIA} + S_{LWS}, \quad (1)$$

where S_{TOT} is the change in mean sea level for each component since the base period. S_{OCEAN} refers to ocean changes, S_I to ice mass change, S_{GIA} to vertical land movements, and S_{LWS} to anthropogenic land water storage.

Uncertainty and confidence in the quantitative ranges of individual terms are assessed using a variety of techniques, including model-based approaches, expert judgment, and literature review. Subsequent sections describe the basis for projections of each component in greater detail.

B.2 Ocean changes

For NPCC2, future thermosteric and dynamic ocean changes are determined using outputs (the variables ZOSTOGA and ZOS in the CMIP5 archive) from 24 CMIP5 GCMs under both RCP4.5 and RCP8.5 (see later), yielding a total of 48 outcomes. As in Yin *et al.* (2012), dynamic sea level is now defined as the grid point anomaly from the global mean field.

$$S_{OCEAN} = \mathrm{ZOSTOGA}_t - \mathrm{ZOSTOGA}_{tbase} + \mathrm{ZOS}_t - \mathrm{ZOS}_{tbase}, \quad (2)$$

ZOSTOGA = global mean sea level rise due to thermal expansion, relative to a 2000 to 2004 baseline;
ZOS = local sea level rise due to changes in dynamic ocean height (caused by changes in local ocean density and circulation), relative to the 2000 to 2004 local mean.[d]

Projections of ZOS, particularly the 75th and 90th percentile, reflect a local sea level rise greater than the global mean. This local anomaly has been linked to a slowdown of the Gulf Stream/Atlantic Meridional Ocean Circulation (AMOC) in some GCMs[e] (Yin *et al.*, 2009, 2010; Hu *et al.*, 2009; 2011).

[b]This Appendix provides technical details for New York City Panel of Climate Change 2015 Report, Chapter 2: Sea Level Rise and Coastal Storms.

[c]For example, the NPCC2 approach does not consider whether our estimated 90th percentile land-based ice loss, through its effects on the Gulf Stream, might be inconsistent with a 90th percentile increase in relative ocean height (as estimated using global climate models that do not include the possibility of large land-based ice loss) along the Northeast coast.

[d]Given time constraints and metadata limitations, it was difficult to ascertain whether all modeling centers used the same definitions for zos and zostoga, respectively. For example, at least one model in the CMIP3 archive allowed globally averaged zos to vary in time, while the majority of models did not. Inconsistent definitions of zos and zostoga could lead to inconsistencies in the resulting ocean change term. In general such inconsistencies are expected to have a small effect on the sea level rise projections.

[e]Sea levels are lower to the west of the Gulf Stream than to the east. If the Gulf Stream weakens, a compensating increase in sea level along the Northeast coast is expected; this is an example of a dynamical, or motion related, change in sea level.

Table B.1. New York metropolitan region sea level rise and land subsidence

Station	NOAA SLR (in/year)[a]	Years	PSMSL SLR (in/year)[b]	Years	Peltier GIA (in/year)[c]	Englehart (2009) Paleo-SLR (in/year)[d]	Engelhart & Horton (2012 Paleo-SLR (in/year)[d]
New London	0.10	73	0.10	68	0.04	0.04	~0.04
Bridgeport	0.11	47	0.10	43	0.04	0.04	~0.04
Montauk	0.12	64	0.12	53	0.05	0.03	~0.04
Port Jefferson	0.10	35	0.09	31	0.05	0.03	~0.04
Willets Point	0.10	80	0.10	65	0.05	0.03	~0.04
The Battery/New York City	0.11	155	0.11	138	0.05	0.05	~0.05
Sandy Hook	0.16	79	0.16	79	0.05	0.06	~0.06
Atlantic City	0.16	100	0.16	100	0.05	0.05	~0.06

[a]http://tidesandcurrents.noaa.gov/sltrends/index.shtml/ (see: updated mean sea level trends; current through 2011).
[b]http://www.psmsl.org/products/trends/trends.txt/ (posted January 16, 2013).
[c]GIA corrections for tide gauges predicted by W.R. Peltier's ICE 5G v 1.3, VM2, with 90 km lithosphere resolution. http://www.psmsl.org/train˙and˙info/geo.signal/gia/peltier/drsl250.PSMSL.ICE5Gv1.3˙VM2˙L90˙2012b/ (posted August 13, 2012).
[d]Engelhart *et al.* (2009).
[e]Engelhart and Horton (2012).

A higher-than-average rate of local sea level rise has also been observed in recent decades. Tide gauges along the Atlantic coast show a distinct regional sea level acceleration "hotspot" from Cape Cod to Cape Hatteras since the early 1990s (Sallenger *et al.*, 2012; Boon, 2012; Ezer and Corlett, 2012), although the record is still too short to attribute to climate change because of high interannual to multidecadal ocean variability.

B.3 Ice mass change

In NPCC2, sea level rise contributions from four separate ice masses—the Greenland (GR), West Antarctic (WAIS), and East Antarctic (EAIS) ice sheets, and small glaciers and ice caps (GICs)—are projected independently. At each percentile (10th, 25th, 75th, and 90th), the sea level rise due to changes in ice mass balance at New York City (S_I) is given by the sum of mass changes in each component (where M_x is expressed in sea level equivalent (360 gigatonne mass loss = 1 mm sea level rise) and f_x is the local "fingerprint" of ice mass loss):

$$S_I = -(f_{GIC} M_{GIC} + f_{GR} M_{GR} + f_{WAIS} M_{WAIS} + f_{EAIS} M_{EAIS}). \quad (3)$$

The subsections below discuss the projections of the individual terms in Eq. (3) in more detail.

Mass balance of the Greenland and Antarctic ice sheets. Processes that modify continental ice sheet mass balance (and thus their effect of sea level) can be segregated into those that act on an ice sheet's surface mass balance (or SMB, including snow accumulation, melting, and sublimation) and those that affect ice flow (dynamic changes). Recent observations indicate that dynamic changes underlie virtually all of recently observed mass changes in Antarctica, and approximately half in Greenland (Rignot *et al.*, 2011).

Because robust, process model-based projections of ice sheet contributions to sea level rise are still under development and a complete quantitative assessment is currently unavailable, NPCC2 utilizes the projections of Bamber and Aspinall (2013) for the Greenland and Antarctic ice sheets. Although this study relies exclusively on expert elicitation, it provides a consistent, probabilistic approach for each ice sheet that includes a combined estimate of uncertainty in SMB and ice dynamics.

Mass balance of glaciers and small ice caps[f]. Projections of the future sea level rise contribution of

[f]Uncertainty exists in the assignment of percentiles of GICs.

Box B.1. What is glacial isostatic adjustment (GIA)?

GIAs derive from changes in the size of large ice masses, which distort the Earth's lithosphere and change the elevation of the land surface relative to the ocean. Regions formerly beneath ice sheets around 20,000 years ago (e.g., central Canada and Scandinavia) are still uplifting, while peripheral regions (e.g., New York down to Chesapeake Bay) are subsiding in response to the slow, viscous component of glacial isostatic rebound.

GIA models (such as ICE-5G v1.3 VM2˙L90; Peltier, 2012, 2004; see also Mitrovica and Milne, 2003) calculate gravitational interactions among ice sheets, land, and ocean over time and separate effects of glacial loading/unloading on sea level from the climatic signal. Specific GIA corrections[a] for NYC area tide gauges are listed in Table B.1.

[a]NOTE: These GIA corrections apply to the last deglaciation, not to future ice melting.

GICs have been made using: (1) extrapolations of observed rates of mass change (Bahr *et al.*, 2009); (2) regional, process-based, mass balance models forced by GCMs (Radic *et al.*, 2013; Marzeion *et al.*, 2012), and (3) a statistical approach, whereby mass or volume changes are parameterized as a function of climate (e.g., global mean temperature; Perrette *et al.*, 2013, and references therein). We use the process-based approach of Radic *et al.* (2013) and Marzeion *et al.* (2014), since it does not rely on stationarity as the climate system, and the GICs, evolves over this century.

Fingerprints. Land-based ice compresses the lithosphere, exerts a gravitational pull on the surrounding ocean, and alters the Earth's rotation. Localized ice mass changes thus give a spatially varying pattern of sea level change that is known as a "fingerprint" (Tamisiea and Mitrovica, 2011; Mitrovica *et al.*, 2009, 2001; see Eq. (3)).

For NPCC2, the value of the fingerprint for each ice component in New York City is included as a multiplier of mass change. Here, we assign a single value estimated from the literature (e.g., Mitrovica *et al.*, 2009; Perrette *et al.*, 2013; Gomez *et al.*, 2010; Miller *et al.*, 2013).

B.4 Vertical land movements—glacial isostatic adjustment (GIA)

Vertical land motion in New York City today is primarily "slow" GIA-related subsidence (see Box B.1). Other causes of local vertical land movements (neotectonic activity, sediment loading and compaction, and subsidence due to excess subsurface fluid withdrawal) are expected to remain negligible at the Battery in New York City.

NPCC2 calculates the future subsidence due to GIA as a linear trend where S_{GIA} is the number of years since the start date ($t_{base,}$ 2002, average of 2000–2004) times the annual subsidence rate, R, in mm/year:

$$S_{GIA} = (t - t_{base}) \times R. \quad (4)$$

Table B.1 lists annual subsidence rates, R, for individual tide stations in the New York metropolitan area. Current GIA-related subsidence rates are now much improved over earlier values and compare favorably with millennial sea level rise trends in this region (Engelhart and Horton, 2012; Engelhart *et al.*, 2009). Therefore, $R = 1.26$ mm/year for New York City is used to calculate S_{GIA}. This is roughly 40% of the sea level rise in the observed period.

For historical sea level rise trends, see http://tidesandcurrents.noaa.gov/sltrends/index.shtml/. Updated mean sea level rise trends (current through 2011) for each of the New York metro area tide gauge stations are listed in Table B.1.

B.5 Anthropogenic land water storage

Continental water storage fluctuates due to variability in precipitation, and increasingly since the 1950s due to human interventions in the hydrological cycle. By storing water on land, reservoirs have reduced sea level rise by 0.55 mm/year since the 1950s (Chao *et al.*, 2008) and 0.44 mm/year since the 1970s (Church *et al.*, 2011). Conversely, groundwater mining (water withdrawal in excess of natural recharge) raises sea level.

We also adopted the IPCC (2013) approach in calculating the contribution of changes in land water storage to sea level rise (Church *et al.*, 2013). Specifically, the NPCC 10th, 25th, 75th, and 90th percentile distribution points were calculated by

assuming that IPCC projections of sea level rise are based on a normal distribution. The land water storage rates were treated as linear over time; therefore, the 2020s, 2050s, and 2080s projections could be calculated directly from the IPCC timeslices.

References

Bahr, D.B., M. Dyurgerov & M.F. Meier. 2009. Sea level rise from glaciers and ice caps: a lower bound. *Geophys. Res. Lett.* **36:** L03501, doi:10.1029/2008GL036309.

Bamber, J.L. & W.P. Aspinall. 2013. An expert judgment assessment of future sea level rise from the ice sheets. *Nature Clim. Change* **3:** 424–427.

Boon, J.D. 2012. Evidence of sea level acceleration at U.S. and Canadian tide station, Atlantic Coast, North America. *J. Coast. Res.* **28:** 1437–1445.

Chao, B.F., Y.H. Wu & Y.S. Li. 2008. Impact of artificial reservoir water impoundment on global sea level. *Science* **320:** 212–214.

Church, J.A., P.U. Clark, A. Cazenave, *et al.* 2013. Sea level change." In *Climate Change 2013: The Physical Science Basis. Contribution of Working Group I to the Fifth Assessment Report of the Intergovernmental Panel on Climate Change*. T.F. Stocker, D. Qin, G.-K. Plattner, M. Tignor, S.K. Allen, J. Boschung, A. Nauels, Y. Xia, V. Bex, P.M. Midgley, Eds.: 1137–216. Cambridge, UK: Cambridge University Press.

Church, J.A., *et al.* 2011. Revisiting the earth's sea-level and energy budgets from 1961 to 2008. *Geophys. Res. Lett.* **38:** L188601.

Engelhart, S.E., *et al.* 2009. Spatial variability of late Holocene and 20th century sea-level rise along the Atlantic coast of the United States. *Geology* **37:** 1115–1118.

Engelhart, S.E. & B.P. Horton. 2012. Holocene sea level database for the Atlantic coast of the United States. *Quater. Sci. Rev.* **54:** 12–25.

Ezer, T. & W.C. Corlett. 2012. Is sea level rise acceleration in the Chesapeake Bay? A demonstration of a novel new approach for analyzing sea level data. *Geophys. Res. Lett.* **39:** L19606, doi: 10.1029/2012GL053435.

Gomez, N., J.X. Mitrovica, P. Huybers, & P.U. Clark. 2010. Sea level as a stabilizing factor for marine-ice-sheet grounding lines. *Nature Geosci.* **3:** 850–853.

Horton, R., Rosenzweig, C., Gornitz, V., Bader, D., & O'Grady, M. 2010. Climate Risk Information. In "Climate Change Adaptation in New York City: Building a Risk Management Response. New York City Panel on Climate Change 2010 Report", Rosenzweig, C. and Soleski, W, Eds. *Ann. N.Y. Acad. Sci.* **1196:** 147–228.

Hu, A., G.A. Meehl, W. Han & J. Yin. 2009. Transient response of the MOC and climate to potential melting of the Greenland ice sheet in the 21st century. *Geophys. Res. Lett.* **36:** L10707.

Hu, A., G.A. Meehl, W. Han & J. Yin. 2011. Effect of the potential melting of the Greenland Ice Sheet in the Meridional Overturning Circulation and global climate in the future. *Deep-Sea Res. II* **58:** 1914–1926.

IPCC. 2013. *Climate Change 2013: The Physical Science Basis. Contribution of Working Group I to the Fourth Assessment Report of the Intergovernmental Panel on Climate Change*. Stocker, T.F., D. Qin, G.-K. Plattner, M. Tignor, S.K. Allen, J. Boschung, A. Nauels, Y. Xia, V. Bex and P.M. Midgley, Eds: Cambridge University Press Cambridge, United Kingdom and New York, NY, USA, 1535 pp

Marzeion, B. A.H. Jarosch, & M. Hofer. 2012. Past and future sea-level change from the surface mass balance of glaciers. *Cryosphere* **6:** 1295–1322.

Marzeion, B., J. G. Cogley, K. Richter, and D. Parkes. 2014. Attribution of global glacier mass loss to anthropogenic and natural causes. *Science* **345:** 919–921.

Miller, K.G., R.E. Kopp, B.P. Horton, *et al.* 2013. A geological perspective on sea-level rise and its impacts along the U.S. mid-Atlantic coast. *Earth's Future* **1:** 3–18.

Mitrovica, J.X. & G.A. Milne. 2003. On post-glacial sea level: I. General theory. *Geophys. J. Int.* **154:** 253–267.

Mitrovica, J.X., M.E. Tamisiea, J.L. Davis, & G.A. Milne. 2001. Recent mass balance of polar ice sheets inferred from patterns of global sea-level change. *Nature* **409:** 1026–1029.

Mitrovica, J.X., N. Gomez & P.U. Clark. 2009. The sea-level fingerprint of West Antarctic collapse. *Science* **323:** 753.

NPCC. 2010. Climate Change adaptation in New York City: building a risk management response. New York City Panel on Climate Change 2010 Report. C. Rosenzweig and W. Solecki, Eds. *Ann. N.Y. Acad. Sci.* **1196:** 1–354.

NPCC. 2015. Building the Knowledge Base for Climate Resiliency: New York City Panel on Climate Change 2015 Report. C. Rosenzweig and W. Solecki, Eds. *Ann. N.Y. Acad. Sci.* **1336:** 1–149.

Peltier, W.R. 2012. GIA data sets. http://www.psmsl.org/train_and_info/geo_signals/gia/peltier/drs250.PSMSL.ICE5GV1.3_VM2_L90_2012b.txt. Accessed March 1, 2013.

Peltier, W.R. 2004. Global glacial isostasy and the surface of the ice-age earth: the ICE-5G (VM2) Model and GRACE. *Annu. Rev. Earth Planet. Sci.* **32:** 111–149.

Perrette, M., F. Landerer, R. Riva, K. Frieler, & M. Meinschausen. 2013. A scaling approach to project regional sea level rise and its uncertainties. *Earth Syst. Dyn.* **4:** 11–29.

Radic, V., A. Bliss, A.C. Beedlow, *et al.* 2013. Regional and global projections of twenty-first century glacier mass changes in response to climate scenarios from global climate models. *Clim. Dyn.*: **42:** 37–58.

Rignot, E., I. Velicogna, M.R. van den Broeke, *et al.* 2011. Acceleration of the contribution of the Greenland and Antarctic ice sheets to sea level rise. *Geophys. Res. Lett.* **38:** L05503. doi:10.1029/2011GL046583.

Sallenger, A.H., Jr., K.S. Doran & P.A. Howd. 2012. Hotspot of accelerated sea-level rise on the Atlantic coast of North America. *Nature Clim. Change* **2:** 884–888.

Tamisiea, M.E. & J.X. Mitrovica. 2011. The moving boundaries of sea level change: Understanding the origins of geographic variability. *Oceanography* **24:** 24–39.

Yin, J., M.E. Schlesinger & R.J. Stouffer. 2009. Projections of rapid sea-level rise on the northeast coast of the United States. *Nature Geosci.* **2:** 262–266.

Yin, J., S.M. Griffies & R.J. Stouffer. 2010. Spatial variability of sea level rise in twenty-first century projections. *J. Clim.* **23:** 4585–4606.

Yin, J. 2012. Century to multi-century sea level rise projections from CMIP5 models. *Geophys. Res. Lett.* **39:** L17709.

C. Static coastal flood mapping[g]

Contents

C.1 United States Army Corps of Engineers hurricane storm surge inundation areas
C.2 NPCC2 baseline flood elevation datasets
C.3 line flood elevation datasets: Lateral variations
C.4 Baseline flood elevation datasets: Rounded integer values
C.5 Vertical datum
C.6 Vertical accuracy of elevation data
C.7 Future work: Mapping uncertainty in the elevation dataset
C.8 Future work: Combined uncertainties

This section includes technical material supplementary to Chapter 3, Static Coastal Flood Mapping (NPCC, 2015). It was created to add detail about the mapping methodology and limitations, datasets, and accuracy issues that were touched upon in the main chapter.

C.1 United States Army Corps of Engineers hurricane storm surge inundation areas

The United States Army Corps of Engineers (USACE) develops storm surge inundation maps from the National Hurricane Center's SLOSH (Sea, Lake, and Overland Surges from Hurricanes) model.

The NYC Office of Emergency Management (OEM) uses these inundation maps to understand worst-case scenario storm surge in New York City to develop the city's evacuation zone maps. Storm surge inundation zones are delineated for hurricane categories 1–4, with six possible bearings, ranging from Northeast (NE) to West North West (WNW). The bearing is the direction in which the hurricane is headed. OEM uses two SLOSH products, MEOWs (Maximum Envelope of Water) and MOMs (Maximum of MEOWs), in its planning and preparedness efforts. The MEOW is based on a set of storms with fixed intensity and bearing, but with varying sizes, forward speeds, and landfall locations. Surge inundation zones based on the MEOWs were used to create New York City's hurricane evacuation zones, which are the primary tool for communicating the surge hazard to the public. Surge inundation zones created from the MOMs are used to plan for the worst-case inundation for a category of hurricane without regard to the probability of occurrence. The SLOSH data used for OEM's planning assume that the hurricane makes landfall at high tide.

C.2 NPCC2 baseline flood elevation datasets

Base flood elevations (BFEs) and still-water elevation (SWEL) data from FEMA's Preliminary Flood Insurance Study (FIS) and FIRMs serve as the baseline to which projections of sea level rise were added to create maps of the future 100- and 500-year flood scenarios. The 500-year SWEL raster was calculated by FEMA and their mapping partners using the Advanced Circulation Model for Oceanic, Coastal and Estuarine Waters (ADCIRC) coupled to the unstructured numerical wave model Simulating Waves Nearshore (unSWAN), referred to as SWAN + ADCIRC hydrodynamic models (FEMA, 2013). This modeled output of SWELs considers the projected elevation of floodwaters in the absence of wave heights and wave runup, but with consideration of wave setup.[h]

The 100-year coastal BFEs are founded on 100-year SWEL data, and then wave height (derived through the Wave Height Analysis for Flood Insurance Studies (WHAFIS) model) and wave runup (derived through various runup models, where applicable) were incorporated.[i] The use of the SWEL depth grid (raster) values instead of BFE values for the 500-year flood extent is a departure from the 2013 flood map methodology, in which BFE values were used for both the 100- and 500-year flood maps. Because BFEs incorporating wave heights and wave runup were not calculated for the 2013 Preliminary FIRM 500-year flood extent, 500-year SWEL data were used as a proxy. The older FEMA Advisory BFE values for the 500-year flood (released in

[g]This Appendix provides technical details for New York City Panel of Climate Change 2015 Report, Chapter 3: Static Coastal Flood Mapping.

[h]Wave setup is the increase in the water level caused by the onshore mass transport of water that occurs due to waves breaking during a storm. Wave runup is the rush of water that extends inland when waves come ashore.

[i]FEMA's Flood Insurance Study (FIS) for the city of New York (revised December 5, 2013) details the baseline engineering methods used in determining the 100- and 500-year floodplains. The 2013 FIS revision can be accessed through the FEMA Map Service Center website: https://msc.fema.gov/.

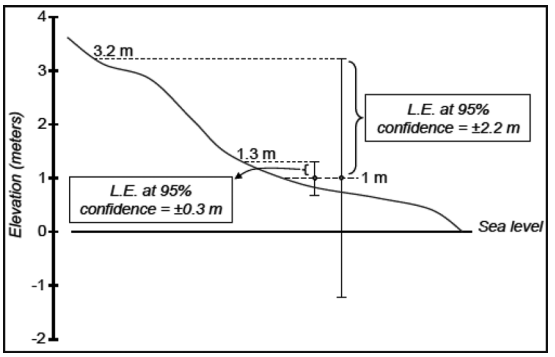

Figure C.1. An example of linear error (L.E.) mapping using two elevation (topographic) models with differing vertical accuracies: one with a 95% confidence interval of 7.2 feet (2.2 m), and the other with a 95% confidence interval of 0.98 feet (30 cm; Source: Gesch, 2009).

February 2013, followed by the Preliminary FIRM dataset released that December) were considered for use, but the 0.2% SWEL data were ultimately selected as the best available data. The 0.2% SWEL data are based on a completely revised coastal modeling analysis for all New York City neighborhoods and approximate BFE values in inland areas where wave action is negligible (A. Martin, 2014, personal communication). Exceptions are areas where wave runup is the dominant coastal process: in these few areas, BFE values exceed 500-year SWEL values by many feet and produce a 100-year flood zone that extends beyond the 500-year projection. For mapping purposes, this issue was resolved by merging the 100- and 500-year datasets such that the runup areas are also included in the 500-year flood extent.

C.3 Baseline flood elevation datasets: Lateral variations

FEMA's BFE and SWEL elevations vary both parallel and perpendicular to the shoreline and thus are not at a constant elevation. The transitions in flood elevation values along the coasts should be reflected in the landward movement of floodwaters, such that the inland shape and extent of the flood zone reflects the changing BFE values nearer to shore. The NPCC approach incorporates these lateral variations in flood elevation values by assuming that landward values of floodwater elevation are likely to be more similar to neighboring flood elevation values and less similar to more distant values. To execute this concept in a geographic information system, Thiessen polygons are created in the coastal area. These polygons define and assign a value to the area closest to a given point relative to all other points in the dataset. They are used to delineate the new boundaries between BFE zones as floodwaters are projected landward. However, by this process, areas of low topography that are not connected to open water will nonetheless appear as islands of flooding among nonflooded terrain. These "orphans" are later removed using spatial selection queries of the raster pixels.

C.4 Baseline flood elevation datasets: Rounded integer values

On FEMA's 2013 Preliminary FIRM for New York City, BFEs are given as values rounded to the nearest whole number (feet). BFEs represent the height (referenced to the NAVD 1988 vertical datum) to which floodwaters will rise during the 100-year flood. On FIRMs they are represented as single-value zones (e.g., "8" or "10" feet); however, they actually represent a range of values. For example, the BFE labeled as 10 feet actually encompasses all values from 9.6 feet to 10.5 feet—a range just larger than the NPCC2 90th percentile sea level rise projection of 10 inches for the 2020s. By contrast, FEMA's SWEL raster elevation dataset (used for the 500-year flood maps) contains values presented as decimals (e.g., 9.6, 9.7); however, in the process of preparing the SWEL data for mapping, the decimals were converted to whole integers by rounding the values. Rounded integer values are less accurate than decimal values and introduce a margin of uncertainty into the future flood map products.

C.5 Vertical datum

It is important that the topographic and floodwater elevations used in the NPCC2 mapping effort are referenced to a common vertical standard in order to create consistency among elevation data. Tidal data, which reference average water levels, and geodetic data, which reference ground-based benchmarks, have both been used to standardize to flood map elevations within a data system. The NPCC2 work references elevation data to the North American Vertical Datum of 1988 (NAVD88).

The east and west coasts of the United States experience semidiurnal tides consisting of two high and two low tides per day. The "higher high water" elevation represents the height of the higher of the two daily high tides and the "lower low water" elevation represents height of the lower of the two daily low tides. The Mean Higher High Water (MHHW)

tidal datum is defined as the average of daily higher high water heights during the current National Tidal Datum Epoch (NTDE; current is 1983–2001). Common practice is to use the MHHW tidal datum as baseline when mapping sea level rise inundation because MHHW represents the highest level of daily inundation (Cooper *et al.* 2013). Despite this convention, the extents of the future flood maps developed by NPCC2 are calculated with reference to NAVD88, a geodetic datum situated 2.5 inches (0.21 feet) above mean sea level and 30 inches (2.5 feet) below MHHW at the Battery NY (at lower Manhattan). The NAVD88 was selected as the NPCC2 baseline because (1) the NYC Digital Elevation Model (DEM) and FEMA FIRMs datasets used in developing the future flood maps are already referenced to NAVD88; and (2) MHHW is not the optimal foundational datum for the purposes of approximating future flood events since sea level rise is a slow and long-term event.

As a gradual decadal process that affects the full tidal cycle at a given location, sea level rise slowly elevates both the mean high and low water levels relative to previous values. For this reason it is practical to map sea level rise inundation onto the highest level of daily inundation, that is, MHHW, to ensure coverage of the fullest extent of daily water level ranges. However, unlike sea level rise inundation, flood events can be very brief, with peak waters often lasting less than a full tidal cycle and do not always occur during high tides. If the flood event is minor or occurs coincident with Mean Lower Low Water (MLLW), water levels may never reach or exceed the height of MHHW. For this reason, using the NAVD88 for mapping reference is appropriate for flood events because NAVD88 approximates mean sea level and does not superimpose the effects of daily tidal cycles on flood elevation.

C.6 Vertical accuracy of elevation data

The topographic dataset used by the NPCC2 was a DEM created from Light Detection and Ranging (LiDAR) data collected in spring 2010 over New York City. Vertical accuracy of this dataset was reported as 9.5 cm root mean square error (RMSE). RMSE is a common method of accuracy reporting[j] calculated as the square root of the average of the set of squared differences between dataset coordinate values and coordinate values from an independent source of higher accuracy (NDEP, 2004). These higher accuracy sources can often include geodetic ground surveys, Global Positioning System ground surveys, photogrammetric surveys, and spatial databases of substantially higher accuracy (ICSM, 2009):

$$\mathrm{RMSE}_Z = \mathrm{sqrt}[\Sigma(Z_{\mathrm{data}i} - Z_{\mathrm{check}i})^{2/n}], \quad (5)$$

where $Z_{\mathrm{data}\,i}$ is the vertical coordinate of the ith checkpoint in the dataset, $Z_{\mathrm{check}\,i}$ is the vertical coordinate of the ith checkpoint in the independent source of higher accuracy, i is an integer from 1 to n, and n is the number of points being checked.

In addition to RMSE, the National Standard for Spatial Data Accuracy (NSSDA) uses the linear uncertainty value at the 95% confidence interval to report vertical accuracy (Federal Geographic Data Committee, 1998). This metric is expressed as:

$$\text{Linear Error at 95\% confidence (LE95)} = 1.96 \times \mathrm{RMSE}_Z. \quad (6)$$

Using Eq. (2) above, the DEM RMSE value of 9.5 cm equates to a linear error at 95% confidence value of 5.3 inches (18.6 cm). Thus the 90th percentile sea level rise projections of 10 inches (25.4 cm) for the 2020s, 30 inches (76.2 cm) for the 2050s, 58 inches (145.3 cm) for the 2080s, and 75 inches (190.5 cm) for 2100 all exceed the 95% error bounds of the elevation data.

C.7 Future work: Mapping uncertainty in the elevation dataset

It is important to convey the vertical uncertainty of the underlying elevation dataset in any flood or inundation mapping exercise. The term uncertainty is used to express a quantitative indication of the quality of elevation data using a specified level of confidence. In topographic elevation data uncertainty is often depicted by one of two techniques. The first is the NSSDA linear error technique mentioned above (Eq. (2), which is based on "... a linear uncertainty value such that the true or theoretical location of the point falls within ± of that linear uncertainty value 95-percent of the time" (Federal Geographic Data Committee, 1998). This calculation of linear error of the topographic data can be depicted on sea level

[j] Accuracy refers to the closeness of a measured value to a standard or known value.

rise inundation maps as a second boundary above or outside the inundation boundary (Fig. C.1; Gesch, 2009, Cooper *et al.*, 2013). In this way the magnitude of uncertainty of the topographic dataset is captured visually as the distance between the sea level rise and linear error boundaries. Greater width between the two indicates greater uncertainty.

In contrast to uncertainty, error refers to the difference between the measured and true values of elevation data. It is reported as the RMSE or Accuracy$_z$ (see Eq (1), which for the purposes of the NPCC2 work, are assumed to be equivalent to the standard deviation and 95% confidence interval, respectively. Mapping uncertainty in the elevation dataset can also be done using a basic equation to compute a standard score, which is the number of standard deviations a value falls from the mean.

$$\text{Standard Score}_{(X,Y)} = (\text{Inundation}_{(\text{watersurface})} - \text{Elevation}_{(X,Y)})/\text{RMSE}_{(\text{ElevationData})}. \quad (7)$$

Standard scores are critical in conveying the accuracy of the elevation data, as mapping an inundation extent can be done with data of any quality irrespective of its accuracy. However, standard-score maps delineate zones of high and low confidence in the elevation data. Standard scores also reflect areas of high and low uncertainty that are independent of data accuracy, but instead are connected to slope; low slopes will have higher uncertainty and areas of high slopes will have lower uncertainty since a large vertical error will result in less of a horizontal error. A given location can also have different uncertainties relative to the level of inundation: a low level of inundation may correspond to an area of low slope, while high inundation at the same location may fall along an area of high slope (NOAA 2010). Future flood map work could use either linear boundary or standard score methods to display the uncertainty in the underlying elevation dataset.

C.8 Future work: Combined uncertainties

In addition to vertical error in the LiDAR dataset, the modeled sea level rise projections for the 2020s, 2050s, 2080s, and 2100, and the FEMA base flood and SWEL datasets upon which the future flood zones are founded, have ranges of error that can also be expressed as confidence intervals. The error in these three sources can be combined into an "uncertainty envelope" and mapped above and below the projected future flood boundary. Several studies have used this probabilistic technique, combining the vertical error of LiDAR elevation data and vertical error of the tidal grids (which are calculated using NOAA's VDatum tool) to give the probability of inundation for a given location at 90% and 95% confidence intervals (Mitsova *et al.*, 2012; NOAA, 2010).

An important disclaimer to the NPCC2 future flood maps is that they are used for illustrative purposes only and should not be used for site-specific planning or insurance requirements. This statement is intended to prevent users from assuming the maps are a perfect representation of projected future flood extents. Future work should attempt to account for the uncertainty in map data sources and products and to illustrate this uncertainty directly on the map as confidence intervals.

References

Cooper, H.M., Q. Chen, C.H. Fletcher & M.M. Barbee. 2013. Assessing vulnerability due to sea-level rise in Maui, Hawai'i using LiDAR remote sensing and GIS. *Clim. Change* **116:** 547–563.

FEMA. 2013. *Flood Insurance Study: City of New York, New York, Bronx County, Richmond County, New York County, Queens County, Kings County*, pp. 131. FEMA.

Federal Geographic Data Committee. 1998.

Gesch, D.B. 2009. Analysis of lidar elevation data for improved identification and delineation of lands vulnerable to sea-level rise. *J. Coast. Res.* **53:** 49–58.

ICSM. 2009. Australian Map and Spatial Data Horizontal Accuracy Standard. Intergovernmental Committee on Surveying and Mapping, pp. 16.

Mitsova, D., A.-M. Esnard, Y. Li. 2012. Using enhanced dasymetric mapping techniques to improve the spatial accuracy of sea level rise vulnerability assessments. *J. Coastal Conservation* **16:** 355–372.

NDEP. 2004. *Guidelines for Digital Elevation Data, Version 1.0.* National Digital Elevation Program. pp. 93.

NOAA. 2010. *Mapping Inundation Uncertainty.* Charleston, NC: NOAA Coastal Services Center.

NPCC. 2015. Building the Knowledge Base for Climate Resiliency: New York City Panel on Climate Change 2015 Report. C. Rosenzweig and W. Solecki, Eds. *Ann. N.Y. Acad. Sci.* **1336:** 1–149.

D. Dynamic coastal flood modeling[k]

Contents

D.1 The FEMA Region II flood mapping study (2014)
D.2 Overland wave heights
D.3 Storm set
D.4 Statistics
D.5 Dynamic coastal flood mapping

D.1 The FEMA Region II flood mapping study (2014)

FEMA recently performed its first complete coastal flood zone reassessment for Region II since 1983 (FEMA, 2014a), and draft maps (2013 Preliminary FIRMs), and the reports are currently out for public comment (http://www.region2coastal.com/). The study used a computer modeling approach for its assessment (e.g., Niedoroda *et al.*, 2010; Toro *et al.*, 2010). Historical storm and sea level data from 1938 to 2009 were used to help define a regional "climatology" of storms that cause coastal flooding, comprising 159 synthetic tropical cyclones (TCs) and 30 historical extratropical cyclones (ETCs). Hydrodynamic modeling was performed with the coupled modeling system ADCIRC (ADvanced CIRCulation model)/SWAN (Booij *et al.*, 1996; Luettich *et al.*, 1992). With ADCIRC/SWAN, wave/hydrodynamic interactions such as wave set-up are included in SWELs.

The FEMA methods were designed not only to make maximum use of the available detailed historical storm data (1938–2009), but also be useful for looking at a wider range of possible events. They are also designed to include small variations on these historical events that are possible with shifts to the tide phase at storm landfall, or variations in TC variables such as wind speed or storm track (FEMA, 2014c; Toro *et al.*, 2010).

The 30 "worst" ETCs over the period 1950–2009 were defined based on ranking storm surge heights from area tide gauges. Retrospective best estimates ("reanalyses") of wind and atmospheric pressure were constructed using observations and models to represent the meteorology of these historical storms. Representing TCs is more difficult as they are rare in the New York metropolitan region, so the historical storms were utilized with a method called Joint Probability Method Optimal Sampling Quadrature (JPM-OS-Q; Toro *et al.*, 2010) that defines a set of 159 synthetic TCs that covers a wider range of events similar to the historical storms (see Fig. 4.1 in NPCC, 2015). Winds and pressure for TCs were developed using idealized parametric models and a detailed boundary layer model (FEMA, 2014b). The maximum water elevation during a storm in this region is strongly affected by the tide phase relative to the time of peak storm surge. This effect was included in the analysis by assigning a random tide phase to the ADCIRC/SWAN simulation of each of the TCs and ETCs.

Each of the 159 TCs was run one time with a random tide phase, but each of the 30 historical ETCs was run two times with different tide phases, totaling 60 ETCs. Each ETC was run once with a random tide phase, and once with that random storm timing offset by 7 days (nearly half a neap-spring tidal period)—this spreads out the "random" phasing so that storms are run on a wider range of tide phases. As a result, the production simulations covered 159 TCs and 60 ETCs—a total of 219 storms (FEMA, 2014c). Extensive details on the storms, grid development guidelines, the model grid, model validation, and quality control are included in the FEMA report (FEMA, 2014a).

D.2 Overland wave heights

The NPCC2 did not simulate overland wave heights using the WHAFIS model, which was part of FEMA's study—the primary vertical flood level results are SWELs, not BFEs. Note that some studies that map the extent of flood zones with sea level rise utilize BFE data (e.g., NPCC, 2013; also 100-year flood zones in chapter 3 of NPCC, 2015), and in areas with large waves (e.g., Staten Island's southeastern shore), this can lead to flood zone boundaries that are substantially further inland than flood zones mapped using SWEL data. However, at most locations in the New York metropolitan region, the spatial difference in the flood zone boundary is negligible.

D.3 Storm set

Storm surge simulations with the ADCIRC/SWAN computer model are computationally intensive, and

[k]This Appendix provides technical details for New York City Panel of Climate Change 2015 Report, Chapter 4: Dynamic Coastal Flood Modeling.

the short 6-month project timetable precluded running all the storms for each future sea level scenario. As a result, methods were also developed for only simulating a subset of the storms, and yet still utilizing the complete hazard assessment technique that accounts for all the storms. Information on these methods and the added uncertainty they cause in the assessment is given in Orton *et al.* (2014). In short, many of the storms in the FEMA assessment did not cause over-land flooding in New York City, and so the modeling was focused primarily on the storms that caused flooding, indicative of 100- to 500-year events.

D.4 Statistics

Temporal maximum water elevation data computed at each location over the entire domain for each storm were utilized for statistical analysis. For each of the 188,390 grid points in the study area, probability distributions of water elevation were built separately for TCs and ETCs. A detailed description of the statistical methods utilized for converting these distributions to flood-exceedance curves (return period vs. water elevation) is found in Orton *et al.* (2014). As a consistency check, NPCC2 results for the baseline flood assessment were verified against FEMA results. The NPCC2 modeling outputs closely reproduced FEMA flood-exceedance curves, generally within two inches (see Fig. 4.3).

D.5 Dynamic coastal flood mapping

Results of the dynamic coastal flood modeling are shown in flood maps for the baseline and future timeslices. They represent the 100- and 500-year SWEL values taken from the flood-exceedance curves for each grid location. The resulting water elevation data were imported into ArcMAP and interpolated (inverse-distance weighting, IDW) to form a raster surface over the entire region (New York City and the New Jersey Harbor regions). The ADCIRC land-surface elevation (essentially a coarse, 70-m resolution DEM) was also interpolated using IDW to the same cell size as the water elevation rasters. The land surface raster was subtracted from each water elevation raster to compute a map (raster) of flood depth, and the zero contour is the boundary of the flood zone.

For comparison to the static flood zone maps, the ADCIRC land-surface elevations were used, and superposition and the bathtub approach were applied to the baseline SWELs using ArcMAP. The flooded areas with hydraulic connectivity to the open water were identified, keeping only these connected areas and removing all isolated areas. Again, the zero contour is the boundary of the flood zone. This work was done using similar methods to the maps presented in chapter 3, using lower resolution.

References

Booij, N., L. Holthuijsen & R. Ris. 1996. The "SWAN" wave model for shallow water. *Coastal Eng. Proc.* **1:** 668–676.

FEMA. 2014a. *Region II Coastal Storm Surge Study: Overview Report.* 15 p. Washington, DC. Federal Emergency Management Agency.

FEMA. 2014b. *Region II Storm Surge Project: Development of Wind and Pressure Forcing in Tropical And Extra-Tropical Storms Report.* 62 p. Washington DC. Federal Emergency Management Agency.

FEMA. 2014c. *Region II Storm Surge Project: Joint Probability Analysis of Hurricane and Extratropical Flood Hazards Report.* 95 p. Washington, DC. Federal Emergency Management Agency.

Luettich, R., J. Westerink & N.W. Scheffner. 1992. ADCIRC: an advanced three-dimensional circulation model for shelves, coasts, and estuaries. Report 1. theory and methodology of ADCIRC-2DDI and ADCIRC-3DL. C. E. R. C. US Army Corps of Engineers, Ed. Vicksburg, MS. US Army Engineer Waterways Experimentation Station.

Niedoroda, A., D. Resio, G. Toro, *et al.* 2010. Analysis of the coastal Mississippi storm surge hazard. *Ocean Eng.* **37:** 82–90.

NPCC. 2013. *Climate Risk Information 2013: Climate Change Scenarios and Maps Report.* 38 p. New York, NY. New York City Panel on Climate Change.

NPCC. 2015. Building the Knowledge Base for Climate Resiliency: New York City Panel on Climate Change 2015 Report. C. Rosenzweig and W. Solecki, Eds. *Ann. N.Y. Acad. Sci.* **1336:** 1–149.

Orton, P., S. Vinogradov, N. Georgas & A. Blumberg. 2014. Hydrodynamic mapping of future coastal flood hazards for New York City, edited, 37 p. Final report prepared for New York City Office of Emergency Management.

Toro, G., A. Niedoroda, C. Reed & D. Divoky. 2010. Quadrature-based approach for the efficient evaluation of surge hazard. *Ocean Eng.* **37:** 114–124.

E. Public health impacts and resiliency[1]

Contents

E.1 Workshop results for coastal storm resiliency
E.2 Workshop results for extreme heat resiliency

Recommendations are presented regarding improving health resiliency to coastal storms and extreme heat events that were distilled from discussions that occurred during the December 13, 2013, NPCC2 Health Workshop held at Columbia University's Mailman School of Public Health.

E.1 Workshop results for coastal storm resiliency

A range of measures are available to improve resiliency before and during extreme coastal storm events. This means refining early-warning and emergency-response mechanisms, as well as strengthening infrastructure, among other things. Here, we summarize suggestions discussed at the December 13, 2013, NPCC Health Workshop held at Columbia University's Mailman School of Public Health. Table E.1 describes the short-term strategies for building resiliency to coastal storms, while Table E.2 outlines the long-term strategies.

E.2 Workshop results for extreme heat resiliency

A range of measures are available to reduce heat-health risks before and during extreme heat events, including enhancing access to air conditioning for vulnerable individuals, urban greening initiatives, and others. Here, we summarize suggestions discussed at the December 13, 2013, NPCC2 Health Workshop held at Columbia University's Mailman School of Public Health. Table E.3 describes the short-term strategies for dealing with health risks to extreme heat, while Table E.4 outlines the long-term strategies.

Table E.1. Shorter term strategies to build resiliency to coastal storm events

- Improve early warning systems.
- Develop visual, map-based, and accessible probabilistic aids for predicting and contextualizing risk.
- Create a system for knowing where vulnerable people are located within the New York metropolitan region.
- Enhance capacity-building and resource planning for community-based organizations to be optimally helpful.
- Encourage residents to develop storm-preparation plans for themselves and for their apartment building or neighborhoods.
- Improve public messaging about: (1) meteorological information and public health, (2) checking in on neighbors, and (3) using community leaders as avenue for messages and checking on people.
- Centralize communication systems, including the utilization of neighborhood groups, in order to distribute reliable information about risks, preparedness, and support.
- Extend communication systems before and after storm season, and include a variety of avenues.
- Implement a continuous training program to reach residents of all cultures.
- Stockpile infrastructure supplies before storm events to allow for speedier repair of damages.
- Assure that the science on sea level rise and storm surge is applied to New York City flood risk maps.
- Develop real-time floor forecasts at fine scales that take into account special vulnerabilities (e.g., transportation, communications, health, and neighborhood).
- Send rapid-response teams to assess impacts and infrastructure problems, including through community groups and social networks.
- Implement a public education program to increase an "awareness of nature."
- Establish more accurate baselines of locational risks, especially waste sites and locational opportunities (e.g., shelters, care centers).
- Run emergency drills and practices to prepare response teams for extreme coastal storm events.
- Identify concentrations of at-risk populations, and target messaging to isolated groups using key messengers.
- Augment preparedness further in advance of extreme storms.
- Work with local industrial businesses and community-based organizations to assess the vulnerability to hazardous exposures (i.e., toxic chemicals) in industrial waterfront neighborhoods and assess the local capacity for implementation.

Source: NPCC2 Health Group Workshop, December 13, 2013.

[1] This Appendix provides technical details for New York City Panel of Climate Change 2015 Report, Chapter 5: Public Health Impacts and Resiliency.

Table E.2. Long-term strategies to build resiliency to coastal storm events

- Incorporate emergency bypasses to connected transportation systems.
- Add more waterway transportation during pre- and postemergency time periods.
- Change building codes to facilitate preparedness (e.g. location of generator fuel).
- Retool and raise wastewater treatment plants to accommodate for projected sea level rise, storm surge, and rainfall.
- Build resilient power sources for critical infrastructure during storm impacts (e.g., shelters, health facilities).
- Keep power grid on by burying lines underground and using emergency electricity repair vehicles that have the ability to move through deep water.
- Infrastructure improvements, such as those that prevent water from entering subways.
- Instill power back-up plans for buildings.
- Keep health care, internet, and cell service functioning during extreme events.
- Research the utility of microgrids.
- Better match at-risk populations and emergency healthcare provision.
- Increase urban floodwater retention between 1.5 and 12 inches.
- Update building standards (e.g., elevate gear).
- Retrofit multifamily housing and industrial areas to maintain minimum habitability and functionality for at least a few days in the wake of extreme storm: boilers, water, power, etc.; prioritize public housing in these scenarios.
- Promote a layered approach to flood adaptation: not just walls, but also zoning changes, microgrids, and building-level adaptations.
- Research and design flood protections that do not worsen public health risk when design heights or protective capabilities are exceeded (e.g., drowning, water quality).
- Introduce city-scale improvements: hospitals, transportation sewage, green infrastructure, and communications systems.
- Implement neighborhood-scale improvements: shelters, communication systems, and emergency generators.
- Recommend and provide assistance for household improvements: fact-sheets on hardening home, financial support for these measures, and having gas and water storage elevated and stockpiled before storms.
- Research and design best practices to prevent the exposure of hazardous substances and toxic chemicals that are stored, transferred, or handled in waterfront industrial areas in the event of severe weather.

Source: NPCC2 Health Group Workshop, December 13, 2013.

Table E.3. Short-term strategies to build resiliency to extreme heat events

- Improve early warning systems (e.g., earlier messaging and text message alerts that warn people to stay inside during heat-wave events).
- Make cooling centers more accessible, especially in high-risk areas.
- Provide air conditioning subsidies for low-income individuals and households.
- Instill community watch programs, such as the *Look-in on a neighbor* program.
- Target heat-risk awareness to the caregivers of vulnerable populations like student athletes, firemen, kids, meals on wheels, and teachers (e.g., pharmacists can attach letters about heat-risk to prescriptions).
- Expand syndromic surveillance networks to more locations in the metropolitan region.
- Allow pets inside of cooling shelters.
- Research how coupled events (e.g., simultaneous extreme heat and power outage) impact behavioral adaptations.
- Implement regulations on thermostat-use and other energy-related conditions to prevent blackout (i.e., for commercial and public buildings).
- Consider scaled responses to prolonged heat waves and complex disasters.
- Offer ongoing and prewarm season vulnerability education (e.g., how to identify if you're especially vulnerable to heat, what to do about it).
- Provide early warning system for electrical brownouts/blackouts (e.g., possibly incorporating SMS-based, GPS-located warning for load reduction).
- Make better use of mobile devices, social media, and mainstream media to disseminate heat warning, a secondary health risks.
- Implement urban-greening initiatives such as green buildings, "greener" rooms, and planting trees.

Source: NPCC2 Health Group Workshop, December 13, 2013.

Table E.4. Long-term strategies to build resiliency to extreme heat events

- Install infrastructure improvements to the power grid.
- Provide air conditioning units to those who need them (i.e., the most at-risk and vulnerable populations).
- Increase access to green spaces, especially in high-risk areas.
- Increase roof albedo (e.g., require or subsidize cool roofs).
- Develop alternative energy sources for cooling.
- Make sure all buildings have windows that can open to allow for proper ventilation and air flow.
- Design buildings for both heat and cold events.
- Encourage behavior shift by having the City "bring" common organizations of high-risk groups to cooling centers in nonemergency times.
- Install more robust electrical infrastructure, especially in vulnerable neighborhoods and public housing
- Combine urban heat-island mitigation (white roofs, greening, etc.), efficiency improvements, and the expansion of load-shaving programs in order to reduce electrical load.
- Research building designs that reduce need for air conditioning to maintain safe indoor temperatures.
- Develop strategies to "throttle" or limit consumers' use of power during peak demand (e.g., via behavior shifts, technical measures, and pricing).
- Apply a combined heat vulnerability index to target urban heat island interventions, and organize before/after health outcome measures once implemented.
- Increase energy efficiency to cope with excess power demand during extreme heat events.
- Switch to greener energy sources (i.e., renewables).
- Raise public awareness through education so that they know how to anticipate, access, and deal with the risks of heat-wave events.
- Relocate hospitals and care centers to the most populous and most vulnerable areas.

Source: NPCC2 Health Group Workshop, December 13, 2013.

F. Indicators and monitoring[m]

Contents

F.1 Inventory of data sources relevant to climate change in New York City
F.2 Extending climate resilience indicators and monitoring to the New York metropolitan region
F.3 Technical and research support for the NYC Cool Roofs Program

F.1 Inventory of data sources relevant to climate change in New York City

The New York metropolitan region has extant monitoring systems that, although they were not put in place specifically for climate resiliency, can now be utilized for this purpose. Table F.1 provides an inventory of some of these existing data sources.

Additional sources of data (and the climate-related variable they track) in the New York metropolitan region include National Weather Service Automated Surface Observing System (ASOS) locations (meteorological variables), the NOAA-CREST NYCMetNet/Urban Atmospheric Observatory (atmospheric observations, NYS DEC (air quality; see Fig. F.1)), the NYCDEP Harbor Survey (water quality), and the Stevens Institute of Technology New York Harbor Observing and Prediction System (NYHOPS; ocean/coastal).

F.2 Extending climate resilience indicators and monitoring to the New York metropolitan region

While New York City has emerged as a global leader in climate change mitigation and resiliency planning, significant gaps remain between the existing indicators and monitoring systems and what will be needed to support climate change efforts. It will be important to (i) expand the spatial domain included in climate change monitoring for New York City, (ii) maintain and, in some cases, increase the observations that support climate indicators, and (iii) better integrate information from numerous agencies and institutions currently conducting climate change–related monitoring. While funding constraints will be a key challenge for the implementation of the first two recommendations, improved coordination between different monitoring programs may allow for the most efficient use of resources and allow for the needed expansion of existing monitoring.

Climate change will have a significant impact on many sectors critical to New York City, including water resources, energy supply and use, transportation, agriculture, ecosystems, and human health (NPCC, 2010). These systems extend beyond city borders, and as a result, in order to assess the multisectoral impacts of climate change on New York City, it will be important to take a regional approach. The New York metropolitan region includes 31 counties in New York, New Jersey, and Connecticut (Rosenzweig and Solecki, 2001).

Integrating across multiple institutions. Although indicators can be produced in an *ad hoc* manner, with agencies developing and using indicators as needed for various risk management and adaptation needs, the development of a more comprehensive indicators and monitoring system would promote cross-agency collaboration and give high-level decision-makers and the public a broader view of key impacts, vulnerabilities, and adaptation responses. Although the potential policy impact of such a system is significant, investments will be needed to set up a sustainable system for collecting raw data from agencies, climate monitoring systems, remote sensing, census and survey data, and other sources, and for transforming them into indicators. Here we review important considerations and design elements for an integrated system to develop and maintain a robust set of climate change indicators.

A first step will be to identify a coordinating unit for the system. This could be located in the Mayor's Office of Sustainability, Mayor's Office of Recovery and Resiliency, or within an agency such as the Department of Environmental Protection or the Office of Emergency Management. However, it would need to be at a high enough level to be able to coordinate across agencies and address risks across sectors. Second, a technical unit for data processing, indicator calculation, and analysis would need to be set up. This could be within the government, but it might be preferable to have this hosted by an independent institution with

[m]This Appendix provides technical details for New York City Panel of Climate Change 2015 Report, Chapter 6: Indicators and Monitoring.

Table F.1. Data sources in the New York metropolitan region

Data source	Stations in the metropolitan region	Variables monitored	Notes
US HCN v. 2.5 (NOAA NCDC)	22 stations	Monthly average temperature, monthly minimum temperature, monthly maximum temperature, precipitation	Well-documented, consistent data. Adjusted for changes to observational methods, siting and other potential sources of bias as described in Menne *et al.* (2009). Data represents the synergistic impacts of climate and urban land management.
GHCN-Daily (NOAA NCDC)	690 stations	Precipitation, snowfall, snow depth, maximum temperature, minimum temperature	Provides the measured variables, length of record, and period of record by station. There are numerous other variables in addition to the five core ones at daily time step.
US Climate Reference Network (NOAA NCDC)	One station (Milbrook, NY, in Dutchess County)	Three independent measurements of temperature and precipitation at each station. Also observes solar radiation, surface skin temperature, surface winds, soil moisture, and soil temperature at five depths, atmospheric relative humidity.	Reference data: climate change without urban influence. Provides 50-year sustainable, high-quality climate observation network.
NEXRAD WSR-88D Radar	Two stations (KDIX in Mount Holly, NJ, and KOKX in Coram, NY)	Spatial and temporal variability and intensity of precipitation.	Short record.

technical expertise in data analysis and management as well as indicator development. Hosts could include a university or a coalition of universities in the city that could jointly set up a technical unit that has the requisite expertise in the types of data to be managed and processed, including climate, environmental, health, and socioeconomic data. The technical unit would need strong skills in stakeholder engagement, data management, data processing (especially geospatial data processing), and statistics.

The coordinating and technical units together would be responsible for managing stakeholder engagement processes to modify the framework and identify suitable indicators. Often indicators identified in stakeholder processes are vague and open to interpretation. Thus, the technical unit would be responsible for developing a methodology for each indicator. This would include technical specifications such as measurement units, source data, geographic coverage, output resolution, frequency of update, type (current status

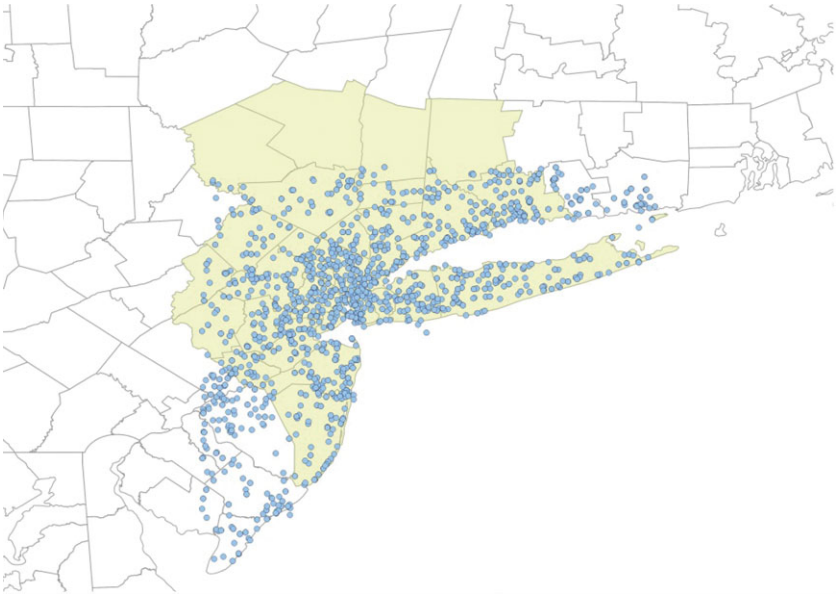

Figure F.1. The 5253 surface meteorological sites that provide data included in the CCNY NYCMetNet Database, which are noted by the blue dots on this map. These sites are operated by multiple public and private institutions.

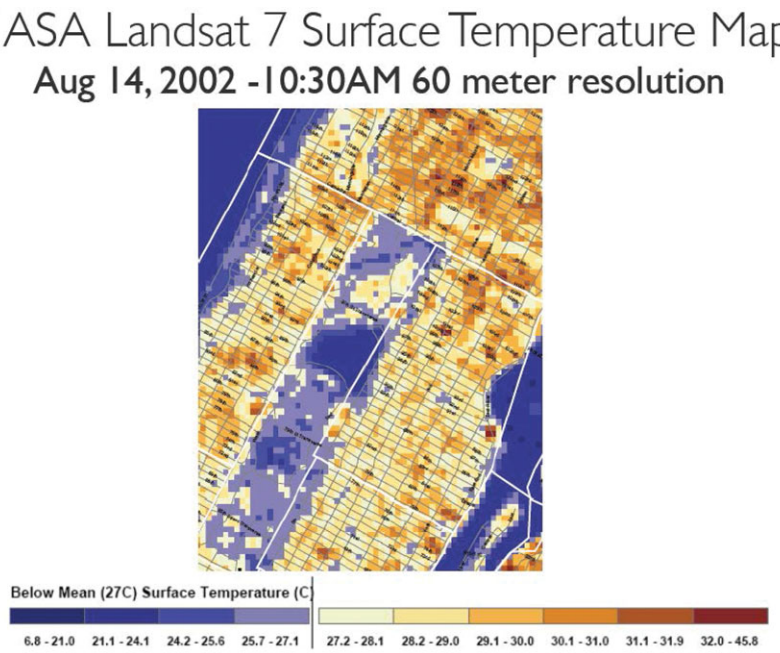

Figure F.2. NASA LANDSAT surface temperature map of Midtown Manhattan with Central Park in the center.

or trend), and statistical transformations needed. This may involve a degree of experimentation with alternative approaches and the production of sample indicators. Once one or more designs/methodologies for each indicator have been developed, it is important to hold a further round of consultations with stakeholders to seek feedback and ensure that the indicators meet user needs. Once agreement is reached regarding a final set of indicators, indicator production methods

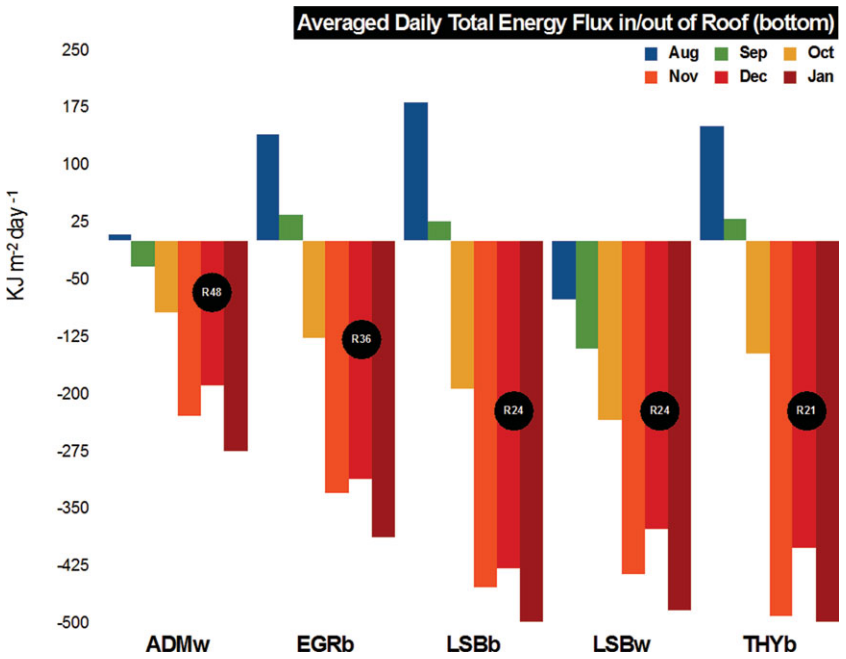

Figure F.3. Measurement of heat gain and loss from five roofs with different colors (albedos) and insulation thicknesses (*R*-values) over buildings in the Princeton Plasma Physic Laboratory.

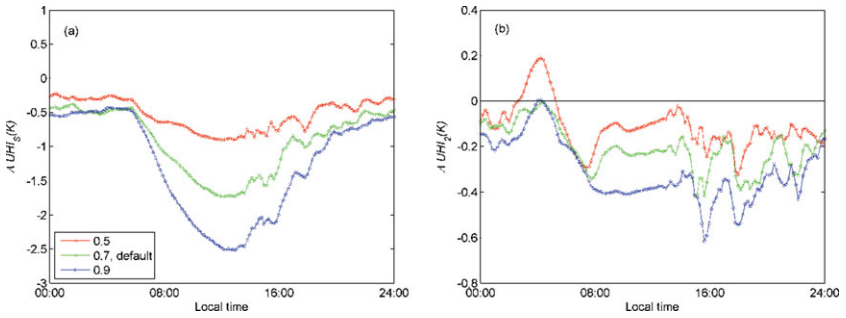

Figure F.4. Impacts of cool roof implementation at the city scale (simulation for Baltimore, MD, from Li *et al.* 2013) as a function of albedo values (the fraction of cool roofs is 50% and the conventional roofs have an albedo value of 0.3). The image on the left shows changes in the surface urban heat island (UHI) and the image on the right shows changes in the near-surface UHI. ΔUHI = $T_{urban} - T_{rural}$ the subscripts are s for surface and 2 for 2 m above surface. The different lines are for albedos of 0.5 (red), 0.7 (green), and 0.9 (blue) as indicated in the legend.

can be standardized and automated to the extent possible.

The technical unit would collate data for the relevant indicators from existing data custodians, with primary sources including city agencies, federal meteorological and climate data managers, climate modeling groups, the U.S. Census, and NASA Centers. Where important indicators are identified but no existing monitoring system exists, the city will need to consider the costs and benefits of adding monitoring systems. The existence of relatively low-cost systems for collecting data (e.g., cheap digital thermometers that can report data wirelessly, which could be placed in a dense network throughout the city), or new crowd-sourcing methods (e.g., for collection of data on the flowering dates of certain plant species or bird migration arrival dates), could mean that costs are in fact quite reasonable.

The coordinating and technical units would be jointly responsible for setting up a Web portal for

indicator reporting, including interactive tools for indicator exploration (map services, data query tools, and data visualization tools). An annual "state of the climate" report could be produced for the city and the wider metropolitan area that summarizes spatial patterns, trends, and results of adaptation efforts, and explains any salient climate phenomena that occurred in that year based on climate indicators. The portal could also include reference information in the form of a bibliographic database searchable by topic, date, geographic scope, and type of climate event.

It must be emphasized that for such a system to be successful, it must not be viewed as an academic exercise, but instead needs to be closely tied to city policy and planning processes.

F.3 Technical and research support for the New York City Cool Roofs Program

Rooftops provide a testbed for studying a number of fundamental urban surface energy balance and climate principles. Indeed, roof scientists and engineers share many concepts and interests with climate scientists, such as weather, climate, extreme events, sunlight and the solar spectrum (including UV radiation, which also can damage membranes), albedo and solar reflectance, temperature cycles, and building energy needs for both heating and cooling. Traditional waterproof roofing systems take many different material forms depending on a number of factors, including local climate conditions, consumer preferences, and historical precedents.

In this section of the appendix, the focus will be on high-albedo roofing for temperature control.

Urban surfaces and rooftop science. Among the many projections of future climate change impacts, ranging from ecological to oceanic to storms and extreme events, increases in heat and heatwave extreme events in urban areas are a great risk. Further, the urban heat island (UHI) is not a disputed concept. Indeed cities are increasingly becoming "crystal balls" into future global warming in so many ways—higher temperatures due to anthropogenic factors, dominant as global sources of CO_2 emissions, vulnerable populations and expensive assets, proactive policies to reduce emissions and develop adaptation, low per capita carbon intensities, and high local ambient atmospheric CO_2 levels.

A major question UHI research faces is how to quantify the relationship between radiometric surface temperature and overlying air temperature, and by how much can ambient air temperatures be lowered by reducing surface temperatures through methods such as increasing albedo and evapotranspiration through the use of new and old green infrastructure technologies.

Rooftops collectively comprise a substantial fraction of land area in urban settings. The percentage varies from city to city, but ranges from 10% to 20% (Rosenzweig *et al.*, 2009). The ubiquitous waterproof rooftop membrane is therefore a fundamental urban surface interacting with the atmosphere and affecting the environment in ways that are increasingly being appreciated and studied.

Among the most salient features of the rooftop environment is that they are hot. During peak sunlight times, membranes can easily reach surface temperatures of 170°F (77°C) (Gaffin *et al.*, 2012). And, such peak temperatures do not require high summertime air temperatures, but are generally much more strongly dependent on incident sunlight conditions; it is sometimes the case that the surface temperatures are even higher during spring rather than summer, when less hazy urban air prevails.

Contrastingly, night-time rooftop surfaces temperatures can drop remarkably low, especially under calm, clear conditions. Nocturnal temperatures as low as −11°F (−24°C) have been observed (Gaffin *et al.*, 2012). The explanation for how temperatures can drop this low has to do with the fact that the rooftop is experiencing net negative longwave radiation imbalance, in that downward longwave radiation is emanating from high tropospheric altitudes with correspondingly low blackbody radiation temperatures. The rooftop is emitting longwave radiation at much higher terrestrial surface temperatures and hence a negative energy imbalance ensues. Under such conditions surface, the surface temperature on the rooftop will keep dropping until it matches the extremely cold high-altitude tropospheric effective longwave radiation temperature. An important contributing factor here is that rooftop mass is also quite low to minimize structural roof dead load, and so there is little internal mass energy that might otherwise slow down the nocturnal cooling.

Whether such extreme nocturnal cooling is occurring on other prototypical urban surfaces such

as pavement, streets, and walls is less well known although it is unlikely to be as strong. One reason is that in these cases the surface materials are quite dense, and considerable internal energy can be stored during the day that is slowly released at night and probably leads to slower nocturnal cooling as compared to roofs. In addition, if not more important, urban streets and walls have a low sky-view factor compared to roofs, meaning they are often receiving longwave radiation from nearby buildings with correspondingly higher terrestrial and blackbody radiative temperatures than the atmosphere.

The general principle involved is that the surface energy balance radiation fluxes, especially in sunlight, are often more important than air temperature in determining surface temperatures. Latent heat and conductive heat flows however can strongly modulate the radiative energy balance (Gaffin *et al.*, 2010).

Such extreme hot and cold membrane temperatures cycles have practical implications for rooftop service life and building energy gains or losses from the roof. The temperature cycles are a major factor in roof membrane wear and tear as they lead to material expansion and contraction cycles. Also, although peak daytime roof surface temperatures can be very hot, this is counterbalanced significantly by the cold nocturnal cycles, resulting in less energy gain during the summer than might otherwise be expected.

Surface temperature versus air temperature. Urban climate scientists take pains to distinguish the difference between material surface temperatures and air temperatures. To the general public, air temperature is more commonly understood as it is the one reported in daily weather reports and the one individuals bear in mind to prepare for daily activities or travel to different climates. However, surface temperature and its extremes are also clearly familiar in many daily experiences, such as walking barefoot on a sunny beach or touching sliding ponds exposed to long periods of sunlight. To scientists, surface temperature has a number of different names, such as "skin," "radiometric," or "black body radiating" temperature.

With respect to urban climate, these two categories of temperature have different roles to play and are both important, though in different ways. Regarding human thermal comfort and building energy use, air temperature is arguably the more relevant indicator as this is the temperature people feel where they live, work, or play outdoors. The primary goal of UHI mitigation is to ultimately lower such air temperatures during extreme heat events.

However climate science does not have technology to lower air temperatures directly on a large scale, such as the size of a city. On small scales there are a number of familiar thermodynamic methods to reduce air temperatures, but ability for cities to deliberately cool large-scale air masses does not exist. In contrast to air temperature, it is very easy to materially control surface temperatures by altering albedo or creating surfaces that can evaporate or transpire water to vapor, that is, using plant–soil systems. By viewing a surface temperature thermal map of a city (Fig. F.1), it is evident that all the surfaces detected by the satellite sensor are anthropogenic and the extreme range of surface temperatures from hot to cold result from their specific land use and surface material choices.

Cool Roof research conducted in 2012 and 2013: Princeton, NJ, and City of Baltimore, MD. The measurement of heat gain and loss from five roofs with different albedos and insulation thickness over buildings in the Princeton Plasma Physic Laboratory reveals that Cool Roofs offer significant advantages in the summer time, while producing very minimal adverse impacts in the winter (Fig. F.2). Comparing, for example, the LSBb and LSBw roofs in Figure F.2, which have the same insulation (*R*-value of 24) but different albedos (LSBw is a white roof with an albedo of 0.65 m; LSBb is black with an albedo of 0.07), one can notice that their winter months heat losses are comparable. However, during the summer, the figure shows that the heat gains over the black roofs are significantly more substantial. In fact, on average over a day, the white roofs do not gain heat in the summer due to their night-time radiative cooling. In addition, one can see that heat gains in the summer are high for the three black roofs (EGRb, LSBb, and THYb) and much lower for the two white roofs (ADWm and LSBw). The difference between winter time and summer time impact of albedo can be attributed to the diurnal cycle of solar radiation. Roof albedo is only an important factor in roofs performance during hours of high insolation where a high albedo can reflect a

large fraction of that radiation. During the summer months, peak heat gains associated with peak cooling loads occur during the longer summer daytime when insolation is high and the impact of albedo is significant, creating large differences between cool and dark roofs. During the winter, insolation occurs over shorter periods and peak heat losses associated with peak heating loads occur during the nighttime, when albedo has no relevance.

Cool roofs have an impact beyond the scale of a single building. If implemented widely throughout a city, they can reduce surface and air temperatures significantly at the city scale. Simulations using the weather and research forecasting (WRF) model over Baltimore show that these reductions depend almost linearly on the fraction of roofs in the city converted to high-albedo surfaces (Li *et al.*, 2014). Figure F.3 shows a reduction of up to 0.9°F (0.4°C) in air temperature with 50% of the roofs converted to an albedo of 0.7. With 100% penetration of roofs across Baltimore, this cooling effect almost doubles.

The NYC Cool Roofs program: regulatory framework. To help decrease the effects of UHI, the NYC Building Code requires that 75% of the roof area or setback surface on buildings permitted on or after July 1, 2009, be coated white or rated as highly reflective by ENERGY STAR®. In addition, alterations involving the recovery or replacement of an existing roof covering shall comply with Section 1504.8 of the New York City Building Code, unless the area to be recovered or replaced is less than 50% of the roof area and less than 500 square feet.

Local Law 21, 2011, amended this to align with LEED requirements. Effective January 1, 2012, existing buildings making alterations that involve the recovery or replacement of an existing roof must use more reflective and emissive materials.

All building and Cool Roof maintenance is the responsibility of the building owner or manager. This information is conveyed at the initial inspection where the overall condition of the roof is evaluated, as well as type of roof, drainage, ponding, and warranty. No roof will be coated through NYC Cool Roofs if a warranty will be jeopardized. An inspection sheet must be signed off by a building operator prior to any work taking place. In addition, for Cool Roofs to be optimally successful, the roofs must be properly maintained and cleaned throughout the year.

Research questions. In addition to the question of temperature relationships, there are many fundamental research questions associated with high-albedo urban surfaces including cool roofs. Some of these questions that could expand the scope of mitigating the UHI in the New York metropolitan region are as follows:

- How much shortwave radiation is reflected and how does albedo and temperature control decline over time?
- What is the effective transmissivity of this light upwards in the atmosphere and what fraction ultimately reaches the top of the atmosphere (TOA)?
- For reflected light escaping the TOA, this creates a negative radiative forcing, and the carbon equivalence for this forcing can, in principle, be calculated. What is that equivalence?
- What land area worldwide is amenable to this benign form of geo-engineering?
- What does this mean regionally and locally for climate control in the face of global warming?
- What is the public acceptance of higher albedo surfaces and roofs (i.e., neutral, low)? How significant is the scattering of light into neighboring buildings?
- Is there a winter heat penalty in colder climates?
- What are the best protocols for measuring albedo, emissivity, and temperatures in real urban settings where shading, for example, can be quite significant?
- Are there positive synergies between cool roofs and other rooftop infrastructure, such as PV and HVAC systems?
- How can the practical challenges to brightening street-level surfaces—such as pedestrian and vehicular usage—be addressed to allow additional urban surfaces like street pavement and sidewalks to be lightened?

References

Gaffin, S.R., M. Imhoff, C. Rosenzweig, *et al.* 2012. Bright is the new black—multi-year performance of high-albedo roofs in an urban climate. *Environ. Res. Lett.* **7:** 014029.

Gaffin, S.R., C. Rosenzweig, J. Eichenbaum-Pikser, *et al.* 2010. *A Temperature and Seasonal Energy Analysis of Green, White, and Black Roofs.* 19 pp. Center for Climate Systems Research, Columbia University.

Li,T., R.M. Horton, and P.L. Kinney. 2013. Projections of seasonal patterns in temperature-related deaths for Manhattan, New York. *Nature Clim. Change* **3:** 717–721.

Li, D., E. Bou-Zeid & M. Oppenheimer. 2014. The effectiveness of cool and green roofs as urban heat island mitigation strategies. *Environ. Res. Lett.* **9:** 055002.

Menne, M.J., C.N. Williams & R.S. Vose. 2009. The U.S. historical climatology network monthly temperature data, version 2. *Bull. Am. Meteorol. Soc.* **90:** 993–1007.

NPCC. 2010. Climate change adaptation in New York City: building a risk management response. New York City panel on climate change 2010 report. C. Rosenzweig and W. Solecki, Eds. *Ann. N.Y. Acad. Sci.* **1196:** 1–354.

Rosenzweig, C., W.D. Solecki, J. Cox, *et al.* 2009. Mitigating New York City's heat island: integrating stakeholder perspectives and scientific evaluation. *Bull. Am. Meteorol. Soc.* **90:** 1297–1312.

Rosenzweig, C. & W. Solecki. 2001. *Climate Change and a Global City: The Potential Consequences of Climate Variability and Change: Metro East Coast.* 224 pp. For the U.S. Global Change Research Program, National Assessment of the Potential Consequences of Climate Variability and Change for the United States, Columbia Earth Institute.